Compressive Sampling Based Energy Detection of Ultra-Wideband Pulse Position Modulation

Shahzad Gishkori, *Student Member, IEEE*, and Geert Leus, *Fellow, IEEE*

***Abstract*—Compressive sampling (CS) based energy detectors are developed for ultra-wideband (UWB) pulse position modulation (PPM), in multipath fading environments so as to reduce the sampling complexity at the receiver side. Due to sub-Nyquist rate sampling, the CS process outputs a compressed version of the received signal such that the original signal can be recovered from this low dimensional representation. Using the principles of generalized maximum likelihood (GML), we propose two types of energy detectors for such signals. The first type of detectors involves the reconstruction of the received signal followed by a detection stage. Statistical properties of the reconstruction error have been used for the realization of such kind of detectors. The second type of detectors does not rely on reconstruction and carries out the detection operation directly on the compressed signal, thereby offering a further reduction in the implementation complexity. The performance of the proposed detectors is independent of the spreading factor. We analyze the bit error performance of the proposed energy detectors for two scenarios of the propagation channel: when the channel is deterministic, and when it is Gaussian distributed. We provide exact bit error probability (BEP) expressions of the CS based energy detectors for each scenario of the channel. The BEP expressions obtained for the detectors working on the compressed signal directly can naturally be extended to BEP expressions for the related energy detectors working on the Nyquist-rate sampled signal. Simulation results validate the accuracy of these BEP expressions.**

***Index Terms*—Compressive sampling, energy detection, pulse position modulation, ultra-wideband impulse radio.**

I. Introduction

DIGITAL communications is witnessing a phenomenal growth in applications which involve signals of very high bandwidth. Impulse-radio (IR) ultra-wideband (UWB) signals are attractive because they offer high user capacity, fine time resolution as well as low probability of interception and detection [1], [2]. A big hurdle in the implementation of IR-UWB systems is the efficiency of the analog-to-digital converters (ADCs). According to the classical Shannon-Nyquist-Whittaker-Kotelnikov sampling theorem [3], [4], a band-limited signal $x(t)$ (i.e., $X(\omega) = 0, |\omega| > \omega_m$) can be determined completely from its samples $x(nT_s)$ if $T_s \leq \pi/\omega_m$. So the sampling rate should be at least twice the highest frequency. Therefore, if the bandwidth of the signal is too high, ADCs can be heavily stressed causing an increase in the power consumption [5], [6]. It could take decades before the ADC technology is fast, precise and low-cost enough for the present-day high-bandwidth applications [7]. On the other hand, it has been described in [3] that most of the signals with large bandwidths have a small rate of information. This property of wideband signals makes them sparse in information which has led to sampling methods based on the amount of information (or the rate of innovation). The combination of sparsity with finite rate of innovation has been described in [8], primarily for the non-discrete domain. Compressive sampling (CS) [9], [10] offers more flexible options to deal with sparse signals in terms of the location of the information and the non-uniformity of the measurements as we shall elaborate upon in subsequent sections. In this paper, we use CS to capitalize on the time domain sparsity of the IR-UWB signals to reduce the sampling rate as well as the implementation complexity of energy detectors.

We consider UWB pulse position modulation (PPM) signals. PPM is advantageous because of its simplicity and the ease of controlling delays [1] but the disadvantage, in the context of UWB signals, is the relatively large bandwidth associated with it, which causes a large number of visible propagation paths [11]. In this paper, we concentrate on noncoherent PPM receiver design through energy detection [12]–[14] and adopt CS for reduced system complexity as well as power consumption. The resulting detection procedure resembles a generalized maximum likelihood (GML) detector. The symbol decision is determined by the pulse position that contains most of the energy. Note that different works on CS in combination with UWB signals have appeared recently, e.g., in [15] for coherent receivers, in [16] for symbol-rate sampling but requiring pre-identification of the channel which was then extended to [17] for channel and timing estimation, in [18] for a GLRT based detector which was then extended to [19] with an effective measurement matrix design but both requiring the transmission of pilot symbols, in [20] for joint time of arrival estimation and data decoding which requires channel estimation, in [21] and [22] to account for narrow-band interference, in [23] and [24] for UWB channel estimation, in [25] for time-delay estimation and in [26] for differential detection of UWB signals. In contrast to previous methods, we present noncoherent UWB detectors. We neither require pre-identification of the channel, nor the transmission of pilot symbols. Most of the previous methods also require signal reconstruction whereas, we present a method which skips this

Manuscript received August 29, 2012; revised January 01, 2013; accepted April 24, 2013. Date of publication April 30, 2013; date of current version July 10, 2013. The associate editor coordinating the review of this manuscript and approving it for publication was Prof. Eduard Axel Jorswieck. This work is supported in part by NWO-STW under the VICI program (project 10382).

The authors are with the Faculty of Electrical Engineering, Mathematics and Computer Science of Delft University of Technology, 2628 CD, Delft, The Netherlands (e-mail: s.s.gishkori@tudelft.nl; g.j.t.leus@tudelft.nl).

Color versions of one or more of the figures in this paper are available online at http://ieeexplore.ieee.org.

Digital Object Identifier 10.1109/TSP.2013.2260747

step altogether. Note that previous examples of detection with compressed symbols can be found in [26] and [27].

Our Contributions:

- We utilize the CS framework to reduce the receiver sampling rate for IR-UWB PPM signals much below the Nyquist rate.
- Using the principles of GML, we develop CS based energy detectors for the signal reconstructed from its compressed samples. We also propose energy detectors which operate on the compressed signal directly and do not need reconstruction.
- We show that the performance of our proposed energy detectors is independent of the spreading factor.
- We provide bit error probability (BEP) expressions for the proposed compressed detectors for a deterministic channel as well as a Gaussian distributed channel. We show that these expressions can be easily modified for the energy detectors based on Nyquist-rate sampling.

Organization: The paper is organized as follows. Section II presents the system model. Section III provides the CS based energy detectors using the GML criteria for the reconstructed signal as well as for the compressed signal without reconstruction. Section IV provides the theoretical BEP expressions for the CS based energy detectors when the channel is considered deterministic. Section V provides the theoretical BEP expressions when the channel is considered to be Gaussian distributed. Finally, Section VI presents the simulations and the concluding remarks are given in Section VII.

Notations: Matrices are in upper case bold while column vectors are in lower case bold; $[\mathbf{x}]_i$ and $[\mathbf{X}]_{i,j}$ depict the ith and (i,j)th element of the vector $\mathbf{x}$ and matrix $\mathbf{X}$, respectively, whereas the range of the elements is specified by the Matlab-style colon $(:)$ operator in the subscript; $\mathbf{I}_N$ is the identity matrix of size $N \times N$, $(\cdot)^T$ is transpose, $\star$ represents convolution, $\otimes$ stands for the Kronecker product, $\hat{x}$ is the estimate of x, $\mathrm{E}\{\cdot\}$ and $\mathrm{Var}\{\cdot\}$ denote expectation and variance, respectively, $p(\cdot)$ represents a probability density function (pdf), $\triangleq$ defines an entity, and $\|\mathbf{x}\|_p = (\sum_{i=0}^{N-1} |[\mathbf{x}]_i|^p)^{1/p}$ is the ℓ_p norm of $\mathbf{x}$; finally, $\mathrm{sign}(x)$ is the sign function which takes values -1 and 1 depending on the polarity of the element x, whereas the function $(x)_+ = x$ if and only if $x > 0$ otherwise $(x)_+ = 0$.

II. System Model

To transmit the kth information symbol, consider an $\mathcal{M}$-ary PPM signal $s_k(t)$ of length T. Every symbol consists of N_f frames, each with frame duration T_f, so that the symbol time is given by $T = N_f T_f$. The motivation for a multiple-frame transmission has been attributed to the federal communications commission (FCC) limits on the signal power spectral density [28]. Repeating a pulse N_f times, reduces the energy of an individual pulse for a constant symbol energy. In PPM, the signal is modulated by delaying the transmitted pulse within a frame. The ease of implementing these delays also reflects the simplicity of PPM. Let the base pulse delay be defined as, $T_{\mathcal{M}} \triangleq T_f/\mathcal{M}$, then the transmitted signal for the kth information symbol $a_k \in \{0, 1, \ldots, \mathcal{M}-1\}$ can be written as $s_k(t) = \sum_{j=0}^{N_f-1} q(t-(j+kN_f)T_f - a_k T_{\mathcal{M}})$, where $q(t)$ is the unit-energy pulse waveform of duration T_q such that $T_q \ll T_{\mathcal{M}}$. If $g(t)$ represents the impulse response of the physical communication channel, then the received signal corresponding to the kth information symbol is given by

$$\begin{aligned} r_k(t) &= s_k(t) \star g(t) + v_k(t) \\ &= \sum_{j=0}^{N_f-1} h(t - jT_f - kT - a_k T_{\mathcal{M}}) + v_k(t). \end{aligned}$$

where $v_k(t)$ is the additive noise corresponding to the kth information symbol and $h(t) \triangleq q(t) \star g(t)$ is the received pulse waveform of duration T_h. We can represent $r_k(t)$ by its Nyquist-rate sampled version. We take N samples per frame period T_f such that N/T_f is equivalent to the Nyquist rate. Let $N_{\mathcal{M}} \triangleq N/\mathcal{M}$ be the integer number of Nyquist-rate samples in each slot, then the sampled received signal corresponding to the kth information symbol in the jth frame is given by

$$r_{k,i}^{(j)} \triangleq r_k(jT_f + iT_f/N) = h_{i-jN-kNN_f-a_k N_{\mathcal{M}}} + v_{k,i}^{(j)}, \quad (1)$$

for $i = 0, 1, \ldots, N-1$, where $h_i \triangleq h(iT_f/N)$ and $v_{k,i}^{(j)} \triangleq v_k(jT_f + iT_f/N)$. We assume that the elements $v_{k,i}^{(j)}$ are independent identically distributed (i.i.d.) zero-mean Gaussian with variance σ^2. The support of h_i is given by $[0, L-1]$, where $L \triangleq \lceil NT_h/T_f \rceil$ (see Fig. 1). Since we want to make the detection process separable in the different frames/symbols, we do not want the received pulses to overlap and thus we require $T_h \leq T_{\mathcal{M}}$ or $L \leq N_{\mathcal{M}}$. We can also write (1) in the following vector form

$$\mathbf{r}_k^{(j)} = \mathbf{u}^{(j)}(a_k, \mathbf{h}) + \mathbf{v}_k^{(j)} \quad (2)$$

where $\mathbf{r}_k^{(j)} \triangleq [r_{k,0}^{(j)}, \ldots, r_{k,N-1}^{(j)}]^T$, $\mathbf{v}_k^{(j)} \triangleq [v_{k,0}^{(j)}, \ldots, v_{k,N-1}^{(j)}]^T$, and $\mathbf{h} \triangleq [h_0, \ldots, h_{L-1}]^T$. Since we assume that the channel does not vary within a symbol period, $\mathbf{u}^{(j)}(a_k, \mathbf{h})$ is the same for every frame, i.e., $\mathbf{u}^{(0)}(a_k, \mathbf{h}) = \mathbf{u}^{(1)}(a_k, \mathbf{h}) = \cdots = \mathbf{u}^{(N_f-1)}(a_k, \mathbf{h}) = \mathbf{u}(a_k, \mathbf{h})$. The $N \times 1$ vector $\mathbf{u}(a_k, \mathbf{h})$ consists of $\mathcal{M}-1$ blocks of zero values and only one block with L nonzero values provided by $\mathbf{h}$. Let $\tilde{\mathbf{h}} \triangleq [\mathbf{h}^T, \mathbf{0}_{(N_{\mathcal{M}}-L)\times 1}^T]^T$, then the structure of $\mathbf{u}(a_k, \mathbf{h})$ can be represented as

$$\mathbf{u}(a_k, \mathbf{h}) \triangleq \left[\mathbf{0}_{a_k N_{\mathcal{M}} \times 1}^T, \tilde{\mathbf{h}}^T, \mathbf{0}_{(\mathcal{M}-a_k-1)N_{\mathcal{M}}\times 1}^T\right]^T$$

which reflects the enormous amount of sparsity present in UWB PPM signals (e.g., the subsequent sparsity pattern of $r_k(t)$ can be seen as in Fig. 1). The covariance matrix of $\mathbf{v}_k^{(j)}$ can be written as $\mathrm{E}\{\mathbf{v}_k^{(j)} \mathbf{v}_k^{(j)T}\} = \sigma^2 \mathbf{I}_N$. We can finally convert (2) in the following symbol level compact form

$$\mathbf{r}_k = \left[\mathbf{1}_{N_f \times 1} \otimes \mathbf{u}(a_k, \mathbf{h})\right] + \mathbf{v}_k \quad (3)$$

where $\mathbf{r}_k \triangleq [\mathbf{r}_k^{(0)T}, \ldots, \mathbf{r}_k^{(N_f-1)T}]^T$, $\mathbf{v}_k \triangleq [\mathbf{v}_k^{(0)T}, \ldots, \mathbf{v}_k^{(N_f-1)T}]^T$ and $\mathbf{1}_{N_f \times 1}$ is a vector of ones of length N_f.

The CS theory implies that the sparse received signal (comprising K basis functions) is operated upon by a certain transform operator which generates M linear measurements of the received signal such that $M \ll N$, where N represents the number of Nyquist-rate samples of the received signal. This process is carried out in the analog domain [7], [29], [30]. Here, we represent this transform operator as an $M \times N$ measurement

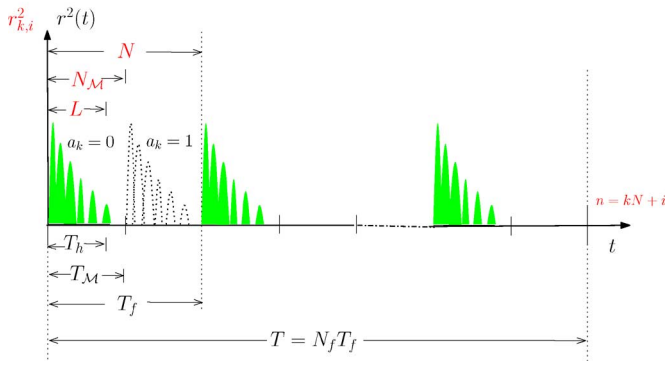

Fig. 1. The squared received signal without noise for $\mathcal{M} = 2$. Labels below the time axis show the usual time-based parameters, while the labels above the time axis show values for the squared Nyquist-rate sampled version of $r(t)$, i.e., $r^2_{k,i}$.

matrix $\mathbf{\Phi}$: $\mathbb{R}^N \longrightarrow \mathbb{R}^M$, with M linear functionals as its rows. Each measurement provides a compressed sample of the received signal which eventually leads to a lower M-dimensional representation of the N-dimensional signal. The ratio between M and N is called the undersampling ratio $\mu \triangleq M/N$. The measurement matrix plays an important role in recovering the signal from its compressed samples. For this, it has to satisfy the restricted isometry property (RIP) [10]. A large number of random matrices, e.g., Gaussian and Bernoulli matrices, as well as structured matrices (with randomly selected rows), e.g., Fourier (for signals with time-domain spasity), satisfy this property.

At this point, we would like to elucidate the structure of the measurement matrix used in the context of our work. To this end, we present the following assumptions.

Assumption 1: The entries of the measurement matrix $\mathbf{\Phi}$ are zero-mean i.i.d. with variance $1/M$. As a result, its covariance matrix can be written as $\mathrm{E}\{\mathbf{\Phi}\mathbf{\Phi}^T\} = \frac{1}{\mu}\mathbf{I}_M$. Now, as $N \longrightarrow \infty$, it can be stated that the rows of the measurement matrix $\mathbf{\Phi}$ are approximately orthogonal to each other, i.e.,

$$\mathbf{\Phi}\mathbf{\Phi}^T \approx \frac{1}{\mu}\mathbf{I}_M. \tag{4}$$

Assumption 2: Considering a $\mathbf{\Phi}$ matrix for which the approximation (4) in Assumption 1 is exact, i.e.,

$$\mathbf{\Phi}\mathbf{\Phi}^T = \frac{1}{\mu}\mathbf{I}_M. \tag{5}$$

In other words, the rows of the measurement matrix are orthogonal and its columns have unit ℓ_2-norm.

Assumption 3: Given a $M_{\mathcal{M}} \times N_{\mathcal{N}}$ matrix $\tilde{\mathbf{\Phi}}$ where $M_{\mathcal{M}} \triangleq M/\mathcal{M}$, in order to treat each of the $\mathcal{M}$ slots separately, the measurement matrix can be designed as $\mathbf{\Phi} = \mathbf{I}_{\mathcal{M}} \otimes \tilde{\mathbf{\Phi}}$.

Note that Assumption 3 can be used along with either Assumption 1 or 2. In the former case, the entries of the matrix $\tilde{\mathbf{\Phi}}$ will be zero-mean i.i.d. with variance $1/M_{\mathcal{M}}$, and in the latter case, the rows of the matrix $\tilde{\mathbf{\Phi}}$ will be orthogonal with unit ℓ_2-norm columns. Assumptions 1 and 2 play an important role in the performance analysis of the proposed detectors. We will explain this in the related sections.

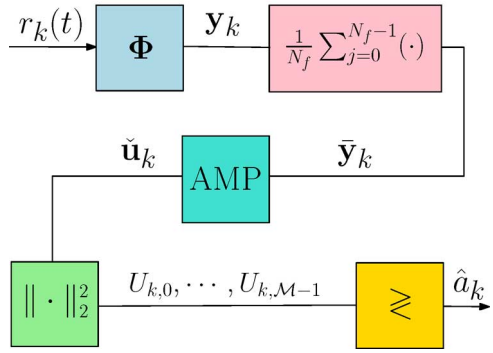

Fig. 2. Block diagram for the CS based ED with reconstructed signals.

Now, applying CS to (2) we can write its compressed version as

$$\mathbf{y}_k^{(j)} \triangleq \mathbf{\Phi}\mathbf{r}_k^{(j)} = \mathbf{\Phi}\mathbf{u}(a_k, \mathbf{h}) + \boldsymbol{\xi}_k^{(j)} \tag{6}$$

where $\mathbf{y}_k^{(j)}$ is the $M \times 1$ measurement vector for the jth frame and $\boldsymbol{\xi}_k^{(j)} \triangleq \mathbf{\Phi}\mathbf{v}_k^{(j)}$ is the $M \times 1$ noise vector. The noise $\boldsymbol{\xi}_k^{(j)}$ is also zero-mean Gaussian with covariance matrix

$$\mathrm{E}\left\{\boldsymbol{\xi}_k^{(j)}\boldsymbol{\xi}_k^{(j)T}\right\} = \mathbf{\Phi}\mathrm{E}\left\{\mathbf{v}_k^{(j)}\mathbf{v}_k^{(j)T}\right\}\mathbf{\Phi}^T \cong \frac{\sigma^2}{\mu}\mathbf{I}_M \tag{7}$$

depending upon Assumption 1 or 2. Note that unlike the commonly used signal models for CS, the noise in our case is also compressed. Thus the choice of the measurement matrix becomes relevant to determine whether the resulting compressed noise is i.i.d. or not. The symbol level joint model can be written as

$$\mathbf{y}_k = \left[\mathbf{I}_{N_f} \otimes \mathbf{\Phi}\right]\mathbf{r}_k = \left[\mathbf{1}_{N_f \times 1} \otimes \mathbf{\Phi}\mathbf{u}(a_k, \mathbf{h})\right] + \boldsymbol{\xi}_k \tag{8}$$

where $\mathbf{y}_k \triangleq [\mathbf{y}_k^{(0)T}, \ldots, \mathbf{y}_k^{(N_f-1)T}]^T$ and $\boldsymbol{\xi}_k \triangleq [\boldsymbol{\xi}_k^{(0)T}, \ldots, \boldsymbol{\xi}_k^{(N_f-1)T}]^T$ are the $N_f M \times 1$ joint compressed measurement and noise vectors for the kth symbol, respectively.

III. CS Based Detection

For low system complexity and power consumption, we focus on the noncoherent reception of UWB PPM signals [12], which is akin to GML detection. The received signal is sampled at a compressed rate according to (6). A straightforward receiver then would require the reconstruction of the actual received signal to carry out the detection process. The other approach may be the detection from the compressed samples directly without reconstructing the received signal. We shall explore both approaches, i.e., the detection after reconstruction and the detection without reconstruction of the compressed received signal (see Figs. 2 and 3 for the block diagrams of the two respective proposed approaches). Either way, we have to handle each frame individually, and we want to find an optimal way to handle multiple frames.

A. Reconstruction Based Detectors

1) Signal Reconstruction and Error Statistics: The reconstruction of a sparse signal calls for the solution of an ℓ_0-norm

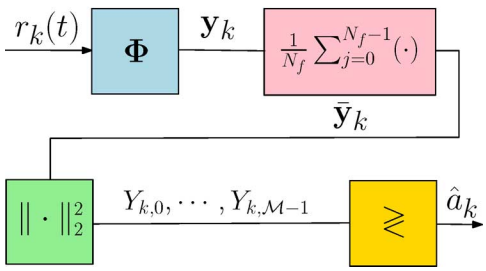

Fig. 3. Block diagram for the CS based ED with compressed signals.

optimization problem. Since the related problem is NP-hard, its ℓ_1-norm equivalent optimization problem, i.e., the convex relaxation of the ℓ_0-norm, has been suggested in the literature [31]. One way to reconstruct the received signal from its compressed samples consists of solving the following optimization problem, (from (8) for $N_f = 1$)

$$\hat{\mathbf{u}}_k = \arg\min_{\mathbf{u}_k} \|\mathbf{u}_k\|_1^1 \quad \text{s.t.} \quad \|\mathbf{y}_k - \mathbf{\Phi}\mathbf{u}_k\|_2^2 \leq \epsilon \tag{9}$$

where $\mathbf{u}_k$ corresponds to $\mathbf{u}(a_k, \mathbf{h})$ and ϵ is a constant. The ℓ_1-norm minimization problem (9), also known as basis pursuit (BP), can recover the sparse signal from its compressed samples but the bottleneck is the size of the signal model. With $N \longrightarrow \infty$, this method becomes computationally expensive (as the worst-case complexity can be of $\mathcal{O}(M^2N^{1.5})$ for interior point algorithms). Alternatively, matching pursuit algorithms can also be used, e.g., orthogonal matching pursuit (OMP) [32], [33] (with a complexity of $\mathcal{O}(KMN)$). These methods are based on iteratively selecting the columns of the measurement matrix, one by one, that are most correlated with the observation vector and its subsequent residual vectors. Variants of matching pursuit algorithms include other greedy algorithms that, in contrast, select more than one column of the measurement matrix through correlations. A case in point is the compressive sampling matching pursuit (CoSaMP) [34] (with a complexity of $\mathcal{O}(MN)$), which also has elaborate performance bounds. In CoSaMP, the signal is estimated by solving a least-squares problem on the candidate components in every step, which involves matrix inversion. This inversion step remains a bottleneck in reducing the computational complexity. The iterative thresholding (ITH) algorithms [35] (with a complexity of $\mathcal{O}(N \log N)$), on the other hand, do not have to invert a matrix, and reconstruct a sparse signal from its compressed samples through the following simple iterations

$$\hat{\mathbf{u}}_k^{[n+1]} = \mathcal{S}\left(\hat{\mathbf{u}}_k^{[n]} + \mathbf{\Phi}^T\mathbf{z}_k^{[n]}, \lambda^{[n]}\right) \tag{10}$$

$$\mathbf{z}_k^{[n]} = \mathbf{y}_k - \mathbf{\Phi}\hat{\mathbf{u}}_k^{[n]} \tag{11}$$

where n is the iteration index and $\mathcal{S}(x, \lambda)$ is the thresholding operator. Variants of ITH are generated depending upon the thresholding to be hard, i.e., $\mathcal{S}(x,\lambda) \triangleq x\mathbb{I}_{\{|x|>\lambda\}}$ (where $\mathbb{I}$ is the indicator function) or soft $\mathcal{S}(x,\lambda) \triangleq \text{sign}(x)(|x| - \lambda)_+$. In general, we will use $\mathcal{S}(x, \lambda)$ to denote a soft thresholding operator. To compare the performance of different ITH algorithms with other approaches e.g., BP or OMP, a performance measure depicting the transitions between success and failure phases of an algorithm, named the sparsity-undersampling (SU) measure, was proposed in [35]. The sparsity $\rho \triangleq \frac{K}{M}$ is the ratio between the number of non-zero components in the sparse signal vector and the number of compressed measurements, whereas the undersampling ratio μ is the ratio between the number of compressed measurements and the total number of elements in the signal vector. Through exhaustive simulations, it was observed in [35] that although ITH is fast and has a low complexity, it unfortunately performs poorly on the SU measure. To retain the fast speed of an iterative algorithm but surpass the performance barrier on the SU measure, the following iterative algorithm, named the approximate message passing (AMP) algorithm, was proposed in [36]–[38]. It can be summarized as

$$\hat{\mathbf{u}}_k^{[n+1]} = \mathcal{S}\left(\hat{\mathbf{u}}_k^{[n]} + \mathbf{\Phi}^T\mathbf{z}_k^{[n]}, \lambda^{[n]}\right) \tag{12}$$

$$\mathbf{z}_k^{[n]} = \mathbf{y}_k - \mathbf{\Phi}\hat{\mathbf{u}}_k^{[n]} + \frac{1}{\mu}\mathbf{z}_k^{[n-1]}\left\langle \mathcal{S}'\left(\hat{\mathbf{u}}_k^{[n-1]} + \mathbf{\Phi}^T\mathbf{z}_k^{[n-1]}, \lambda^{[n-1]}\right)\right\rangle \tag{13}$$

where $\mathcal{S}'(\mathbf{x}, \lambda)$ is the derivative of the soft thresholding operator $\mathcal{S}(\mathbf{x}, \lambda)$ (it generates a 1 for every nonzero element of $\mathbf{x}$) and $\langle\mathbf{x}\rangle$ gives the average value of the elements of $\mathbf{x}$, thus $\langle\mathcal{S}'(\mathbf{x},\lambda)\rangle = \frac{1}{N}\|\mathcal{S}(\mathbf{x},\lambda)\|_0$ where N is the number of elements in $\mathbf{x}$. The key difference between ITH and AMP is the additional term in (13), i.e., $\frac{1}{\mu}\mathbf{z}_k^{[n-1]}\langle\mathcal{S}'(\hat{\mathbf{u}}_k^{[n-1]} + \mathbf{\Phi}^T\mathbf{z}_k^{[n-1]}, \lambda^{[n-1]})\rangle$, altering the residual. In statistical physics, such a term is known as the "Onsager reaction term". For our context and reference we name it as the correction term (CT).

AMP has been derived from the message passing (MP) algorithm which is used in graphical inference models [39]. It was used in [40] for compressed sensing through belief propagation over factor graphs [41]. The problem with the message passing algorithm is that instead of updating only N nodes at each iteration, it updates MN nodes, causing an increase in the computational complexity. If the number of nodes to be updated is restricted to the N variable nodes then message passing reduces to ITH. AMP provides the middle way. By neglecting the weakly dependent updates in the MP algorithm, it updates only N nodes, but what is lost by not updating the M measurement nodes is gained by the addition of the CT. See [37] for a complete derivation of this approximation leading to AMP.

AMP assumes the measurement matrix $\mathbf{\Phi}$ to be a random measurement matrix whose elements are zero-mean i.i.d. with variance $1/M$. In our context, Assumption 1 then becomes relevant. Note, AMP is valid under $N \longrightarrow \infty$. Our Assumption 1 also requires this tendency of N so that (4) can hold. Now, the most important feature of AMP is the statistical characterization of the reconstruction error at every iteration. This can be understood by developing certain heuristics for the iterative approaches. From (11), the correlation of the measurement matrix with the residual vector at the nth iteration can be expanded as

$$\mathbf{\Phi}^T\mathbf{z}_k^{[n]} = \left(\mathbf{u}_k - \hat{\mathbf{u}}_k^{[n]}\right) + \mathbf{H}\left(\mathbf{u}_k - \hat{\mathbf{u}}_k^{[n]}\right) + \mathbf{\Phi}^T\boldsymbol{\xi}_k \tag{14}$$

where $\mathbf{H} \triangleq (\mathbf{\Phi}^T\mathbf{\Phi} - \mathbf{I}_N)$. Now, as described in [36], if it is assumed that $\mathbf{H}$ does not correlate with the vector $\hat{\mathbf{u}}_k^{[n]}$ then

$\mathbf{H}(\mathbf{u}_k - \hat{\mathbf{u}}_k^{[n]})$ can be viewed as a vector of i.i.d. Gaussian random variables and the variance of each variable can be given as $\frac{1}{M}\|\mathbf{u}_k - \hat{\mathbf{u}}_k^{[n]}\|_2^2$. Let the noisy estimate of the received signal be defined as

$$\check{\mathbf{u}}_k^{[n]} \triangleq \hat{\mathbf{u}}_k^{[n]} + \mathbf{\Phi}^T \mathbf{z}_k^{[n]} \tag{15}$$

and the error in estimating the true signal from this estimate be defined as

$$\mathbf{w}_k^{[n]} \triangleq \check{\mathbf{u}}_k^{[n]} - \mathbf{u}_k \tag{16}$$

with $\sigma_w^{[n]2}$ denoting the variance of each of its elements. If the above mentioned heuristics are true, then the variance of the elements of the error vector $\mathbf{w}_k$ can be tracked by the following state evolution (SE) method for every iteration

$$\sigma_w^{[n+1]2} = \Psi\left(\sigma_w^{[n]2}\right) \tag{17}$$

where the function $\Psi(\sigma_w^{[n]2})$ is defined as

$$\Psi\left(\sigma_w^{[n]2}\right) \triangleq \frac{1}{\mu}\left(\sigma^2 + \mathrm{E}\left\{\left\|\mathcal{S}\left(\mathbf{u}_k + \sigma_w^{[n]2}\mathbf{n}, \lambda^{[n]}\right) - \mathbf{u}_k\right\|_2^2\right\}\right) \tag{18}$$

where $\mathbf{n}$ is a vector of zero-mean standard i.i.d. Gaussian random variables, i.e., $\mathbf{n} \sim \mathcal{N}(\mathbf{0}, \mathbf{I}_N)$ and we have considered $\mathrm{E}\{(\mathbf{\Phi}^T\boldsymbol{\xi}_k)(\mathbf{\Phi}^T\boldsymbol{\xi}_k)^T\} = \frac{\sigma^2}{\mu}\mathbf{I}_N$ under Assumption 1. From (18), we can see that the SE also predicts the mean squared error (MSE) of the reconstructed signal in that the SE converges to the true MSE at every iteration as $N \longrightarrow \infty$ [42], i.e.,

$$\mathrm{E}\left\{\left\|\mathcal{S}\left(\mathbf{u}_k + \sigma_w^{[n]2}\mathbf{n}, \lambda^{[n]}\right) - \mathbf{u}_k\right|_2^2\right\} = \frac{1}{N}\left\|\mathbf{u}_k - \hat{\mathbf{u}}_k^{[n]}\right\|_2^2 \tag{19}$$

provided that $\Psi(\sigma_w^{[n]2}) < \sigma_w^{[n]2}$ which should remain true for the SU measure of AMP to coincide with that of other methods, such as BP. It has been observed through extensive numerical simulations (see e.g., [38]) that SE fails to predict the performance of ITH algorithms. The reason is the correlation between $\mathbf{H}$ and $\hat{\mathbf{u}}_k^{[n]}$, which appears right after the first iteration and thus the above heuristics are not true for ITH algorithms. On the other hand, the SE predicts the performance of AMP exactly. The reason is that the CT removes or compensates for the correlation between $\mathbf{H}$ and $\hat{\mathbf{u}}_k^{[n]}$ at every iteration and thus the above heuristics regarding the reconstruction noise being Gaussian and the MSE convergence remain true. Thus the variance of each element of the vector $\mathbf{w}_k^{[n]}$ can be written as

$$\sigma_w^{[n]2} = \frac{1}{\mu}\left(\sigma^2 + \frac{1}{N}\left\|\mathbf{u}_k - \hat{\mathbf{u}}_k^{[n]}\right\|_2^2\right) \tag{20}$$

Note that the performance comparisons described above bring the thresholding policy to the foreground as well. It would suffice to say that the optimal thresholding value should be a function of the standard deviation $\sigma_w^{[n]}$, i.e., $\lambda^{[n]} = \tau\sigma_w^{[n]}$, where τ is a constant. We will describe the thresholding policy used for our purpose in Section VI.

2) GML Based Detection for Multiple-Frame Reconstructed Signals: Let us assume that the received signal was compressed at a compression rate μ and then reconstructed using AMP. Here we assume that the AMP algorithm has reached convergence and therefore drop the iteration indices from the variables. Let $\check{\mathbf{q}}_k$ be a $N_f N \times 1$ vector containing all reconstructed frame vectors $\check{\mathbf{u}}_k^{(j)}$, i.e., $\check{\mathbf{q}}_k \triangleq [\check{\mathbf{u}}_k^{(0)T}, \check{\mathbf{u}}_k^{(1)T}, \ldots, \check{\mathbf{u}}_k^{(N_f-1)T}]^T$. From Section III.A.1, we may assume that the reconstruction error for each signal sample is i.i.d. Gaussian with variance σ_w^2. The pdf for the reconstructed signal from (16) can then be written as

$$p(\check{\mathbf{q}}_k|a_k, \mathbf{h}) = C\exp\left\{-\frac{1}{2\sigma_w^2}\|\check{\mathbf{q}}_k - \left[\mathbf{1}_{N_f\times 1} \otimes \mathbf{u}(a_k, \mathbf{h})\right]\|_2^2\right\} \tag{21}$$

where C is some positive constant. Using the GML criterion, it is clear that in order to maximize (21), we need to minimize the squared ℓ_2-norm, which can be expressed as

$$\begin{aligned}\Lambda(a_k, \mathbf{h}) &= \sum_{j=0}^{N_f-1}\sum_{l=0}^{L-1}\left(h_l^2 - 2h_l[\check{\mathbf{q}}_k]_{P_{j,l}}\right)\\ &= N_f\sum_{l=0}^{L-1}h_l^2 - \sum_{l=0}^{L-1}2h_l\sum_{j=0}^{N_f-1}[\check{\mathbf{q}}_k]_{P_{j,l}},\end{aligned} \tag{22}$$

where $P_{j,l} = jN + a_k N_{\mathcal{M}} + l$ is used for notational simplicity. Taking the partial derivative with respect to h_l while keeping a_k fixed, we obtain

$$\frac{\partial\Lambda(a_k, \mathbf{h})}{\partial h_l} = 2N_f h_l - 2\sum_{j=0}^{N_f-1}[\check{\mathbf{q}}_k]_{P_{j,l}}.$$

Minimizing the cost function with respect to $\mathbf{h}$ would mean setting every gradient with respect to h_l to zero, which yields the following optimal estimate for h_l:

$$\hat{h}_l = \frac{1}{N_f}\sum_{j=0}^{N_f-1}[\check{\mathbf{q}}_k]_{P_{j,l}}. \tag{23}$$

Now substituting (23) in (22), we finally obtain

$$\Lambda(a_k, \hat{\mathbf{h}}) = -N_f\sum_{l=0}^{L-1}\hat{h}_l^2.$$

As a result, the symbol a_k can be found by solving the following problem

$$\min_{a_k}\Lambda(a_k, \hat{\mathbf{h}}) = \max_{a_k}\sum_{l=0}^{L-1}\hat{h}_l^2. \tag{24}$$

Given E_h to be the signal energy per frame, the instantaneous SNR for multiple frames can be defined as $\zeta \triangleq \frac{N_f E_h}{\sigma_w^2}$. From (24) and (23), it can then be observed that for the same instantaneous SNR ζ, the decision result will be independent of the number of frames N_f. This can be explained as follows. The estimate of $\hat{h}_l$ in (23) is obtained by averaging samples over different frames, which on one hand decreases the noise energy by a factor of N_f but on the other hand also decreases the signal energy by a factor of N_f due to the fact that the instantaneous SNR ζ is kept constant [43]. Hence, the performance of the estimate of h_l does not change with N_f and thus also the solution to

(24) does not change with N_f (i.e., the spreading factor) since it only involves the estimate of h_l. Replacing $\hat{h}_l$ in (24) by the value obtained from (23), the optimal energy detector for the reconstructed samples (R-ED) can be written as

$$\hat{a}_k^{(\mathrm{R-ED})} = \max_{a_k} \sum_{l=0}^{L-1} \left[\frac{1}{N_f} \sum_{j=0}^{N_f-1} [\check{\mathbf{q}}_k]_{jN+a_kN_{\mathcal{M}}+l} \right]^2. \quad (25)$$

Replacing the reconstructed samples with Nyquist-rate samples in (25) gives the optimal Nyquist-rate energy detector (N-ED) [43]. So we can see that the optimal procedure consists of first averaging the signal components over different frames and then squaring, and the related performance is independent of the number of frames N_f if the instantaneous SNR ζ is kept constant. This is in contrast to the GML detector proposed in [12] for the Nyquist-rate sampled signal, which consists of first squaring and then averaging. For the reconstructed samples, it can be formulated as

$$\hat{a}_k^{(\mathrm{SR-ED})} = \arg\max_{a_k} \frac{1}{N_f} \sum_{j=0}^{N_f-1} \sum_{l=0}^{L-1} [\check{\mathbf{q}}_k]^2_{jN+a_kN_{\mathcal{M}}+l}. \quad (26)$$

We refer to (26) as the spreading-factor dependent energy detector for the reconstructed samples (SR-ED). Replacing the reconstructed samples with the Nyquist-rate samples leads to the spreading-factor dependent Nyquist-rate energy detector (SN-ED) [12].

3) Averaging Process in the Compressed Domain: We can see that the proposed detection procedure is practically feasible. We avoid Nyquist-rate sampling and the detection is carried out on the reconstructed samples. Still, it may require the reconstruction of all the frames which could be computationally expensive. Here we can benefit from the structure of our compressed detector and save a number of reconstruction steps by reconstructing only one (average) frame instead of all the frames. Since the transform operator $\mathbf{\Phi}$ is the same for all the frames, averaging the reconstructed frames should be similar to averaging the compressed frames and then reconstructing only one average frame. Now, by averaging the compressed frames $\mathbf{y}_k^{(j)}$, for $j = 0, \ldots, N_f - 1$, we can define the compressed average frame by the $M \times 1$ vector $\bar{\mathbf{y}}_k$ as

$$\begin{aligned} \bar{\mathbf{y}}_k &\triangleq \frac{1}{N_f} \sum_{j=0}^{N_f-1} \left(\mathbf{\Phi}\mathbf{u}(a_k, \mathbf{h}) + \boldsymbol{\xi}_k^{(j)} \right) \\ &= \mathbf{\Phi}\mathbf{u}(a_k, \mathbf{h}) + \bar{\boldsymbol{\xi}}_k \end{aligned} \quad (27)$$

where $\bar{\boldsymbol{\xi}}_k = \frac{1}{N_f} \sum_{j=0}^{N_f-1} \boldsymbol{\xi}_k^{(j)}$, and from (4) or (5) the covariance matrix can be written as $\mathrm{E}\{\bar{\boldsymbol{\xi}}_k \bar{\boldsymbol{\xi}}_k^T\} \cong \frac{\sigma^2}{\mu N_f} \mathbf{I}_M$. AMP can help us compare the performance of the two approaches. From (16), we can see that it is sufficient to look at the reconstruction error/noise statistics resulting from the two approaches to assess the performance of the respective detectors. The error variance σ_w^2 in reconstruction via (27) can be written as

$$\sigma_w^2 = \frac{\sigma^2}{\mu N_f} + \frac{1}{\mu N} \left\| \mathbf{u}_k - \hat{\mathbf{u}}_k \right\|_2^2. \quad (28)$$

On the other hand, if each frame is first reconstructed from $\mathbf{y}_k^{(j)}$ with $j = 0, 1, \ldots, N_f - 1$, via AMP and then averaged, the variance of each element of the average noise vector $\bar{\mathbf{w}}_k \triangleq \frac{1}{N_f} \sum_{j=0}^{N_f-1} \mathbf{w}^{(j)}$ can be written as

$$\begin{aligned} \sigma_{\bar{w}}^2 &= \frac{\sigma^2}{\mu N_f} + \frac{1}{\mu N N_f} \sum_{j=0}^{N_f-1} \left\| \mathbf{u}_k - \hat{\mathbf{u}}_k^{(j)} \right\|_2^2 \\ &\approx \frac{\sigma^2}{\mu N_f} + \frac{1}{\mu N} \left\| \mathbf{u}_k - \frac{1}{N_f} \sum_{j=0}^{N_f-1} \hat{\mathbf{u}}_k^{(j)} \right\|_2^2. \end{aligned} \quad (29)$$

Now assuming $\hat{\mathbf{u}}_k \approx \frac{1}{N_f} \sum_{j=0}^{N_f-1} \hat{\mathbf{u}}_k^{(j)}$, (29) is the same as (28). Thus the detectors based on both approaches will perform in a similar manner.

B. Direct Compressed Detectors

In the previous section we looked at detectors based on the reconstructed signals. Here we use GML to develop a detector based on the compressed signals directly, i.e., without reconstruction. Since we have assumed symbol level synchronization, the individual $\mathcal{M}$ pulse positions can also become accessible under Assumption 3. Further, as there is a linear transformation between the actual received signal and its compressed samples, we should be able to segregate the samples of each compressed received frame $\mathbf{y}_k^{(j)}$ for $j = 0, 1, \ldots, N_f - 1$, into $\mathcal{M}$ blocks. Thus, each block would then represent the compressed samples corresponding to a pulse position of the actual received signal. Now considering a measurement matrix $\mathbf{\Phi}$ such that Assumption 2 and 3 hold true, we can write the pdf of the compressed received signal from (8) as

$$\begin{aligned} &p(\mathbf{y}_k | a_k, \mathbf{x}) \\ &\quad = D \exp\left\{ -\frac{1}{2\sigma^2} \left\| \mathbf{y}_k - \left[\mathbf{1}_{N_f \times 1} \otimes \mathbf{\Phi}\mathbf{u}(a_k, \mathbf{h}) \right] \right\|_2^2 \right\} \end{aligned} \quad (30)$$

where D is a constant and $\mathbf{x} \triangleq \tilde{\mathbf{\Phi}}\tilde{\mathbf{h}}$ is an $M_{\mathcal{M}} \times 1$ vector of the compressed samples corresponding to the block in $\mathbf{u}(a_k, \mathbf{h})$ carrying the transmitted pulse. Note that Assumption 2 is important here so that the compressed noise is i.i.d. and (30) can be formulated. Now in order to maximize (30), we need to minimize

$$\begin{aligned} \Lambda(a_k, \mathbf{x}) &= \sum_{j=0}^{N_f-1} \sum_{l=0}^{M_{\mathcal{M}}-1} \left([\mathbf{x}]_l^2 - 2[\mathbf{x}]_l [\mathbf{y}_k]_{P_{j,l}} \right) \\ &= N_f \sum_{l=0}^{M_{\mathcal{M}}-1} [\mathbf{x}]_l^2 - \sum_{l=0}^{M_{\mathcal{M}}-1} 2[\mathbf{x}]_l \sum_{j=0}^{N_f-1} [\mathbf{y}_k]_{P_{j,l}}, \end{aligned} \quad (31)$$

where $P_{j,l} = jM + a_kM_{\mathcal{M}} + l$. Taking the partial derivative with respect to $[\mathbf{x}]_l$ and setting the gradient equal to zero, yields the following estimate for $[\mathbf{x}]_l$

$$[\hat{\mathbf{x}}]_l = \frac{1}{N_f} \sum_{j=0}^{N_f-1} [\mathbf{y}_k]_{P_{j,l}}. \quad (32)$$

Substituting (32) in (31), we get the following compressed samples based energy detector (C-ED)

$$\hat{a}_k^{(\mathrm{C-ED})} = \max_{a_k} \sum_{l=0}^{M_{\mathcal{M}}-1} \left[\frac{1}{N_f} \sum_{j=0}^{N_f-1} [\mathbf{y}_k]_{jM+a_k M_{\mathcal{M}}+l} \right]^2 \quad (33)$$

which is clearly independent of the spreading factor. Thus the energy detector based on the compressed signal directly can be realized by first averaging the compressed samples over the number of frames and then carrying out detection on the average compressed frame directly.

IV. CS Based Detection for a Deterministic Channel

In this section, we consider UWB communications over a deterministic channel. We derive BEP expressions for the CS based detectors when detection is carried out on the reconstructed signal as well as when it is carried out directly on the compressed signal. For simplicity we consider $\mathcal{M} = 2$, i.e., binary PPM.

A. Reconstruction Based Detection

In this section, we derive BEP expressions for the reconstruction based detector. We consider an average compressed frame for reconstruction. Thus the need to reconstruct all the frames has been alleviated except for one average frame. As explained in Section III.A.3, the expressions obtained in this section should also be valid for the detector (25). Again we assume that the convergence stage has been reached for AMP so we will drop the iteration index. We can write the reconstructed symbol as

$$\check{\mathbf{u}}_k = \mathbf{u}(a_k, \mathbf{h}) + \mathbf{w}_k \quad (34)$$

where $\mathbf{w}_k \sim \mathcal{N}(\mathbf{0}, (\frac{\sigma^2}{\mu N_f} + \frac{1}{\mu N}\|\mathbf{u}_k - \hat{\mathbf{u}}_k\|_2^2)\mathbf{I}_N)$ under Assumption 1. Since $\mathcal{M} = 2$, every frame symbol has two pulse positions. Let us assume that the kth symbol is a 0, i.e., $a_k = 0$. This means we transmit the pulse in the first half of the signal frame, and we can partition the reconstructed symbol as

$$\check{\mathbf{u}}_{k,0} \triangleq [\check{\mathbf{u}}(0, \mathbf{h})]_{1:N/2} = \tilde{\mathbf{h}} + \tilde{\mathbf{w}}_{k,0} \quad (35)$$

where $\tilde{\mathbf{w}}_{k,0} \triangleq [\mathbf{w}_k]_{1:N/2}$, and

$$\tilde{\mathbf{u}}_{k,1} \triangleq [\check{\mathbf{u}}(0, \mathbf{h})]_{(N/2+1):N} = \tilde{\mathbf{w}}_{k,1} \quad (36)$$

where $\tilde{\mathbf{w}}_{k,1} \triangleq [\mathbf{w}_k]_{(N/2+1):N}$. Now the GML based detector can be written as

$$U_{k,0} \underset{1}{\overset{0}{\gtrless}} U_{k,1} \quad (37)$$

where

$$U_{k,0} \triangleq \|\tilde{\mathbf{u}}_{k,0}\|_2^2 = E_h + 2\tilde{\mathbf{h}}^T \tilde{\mathbf{w}}_{k,0} + \|\tilde{\mathbf{w}}_{k,0}\|_2^2 \quad (38)$$

with $E_h \triangleq \|\tilde{\mathbf{h}}\|_2^2$ and

$$U_{k,1} \triangleq \|\tilde{\mathbf{u}}_{k,1}\|_2^2 = \|\tilde{\mathbf{w}}_{k,1}\|_2^2. \quad (39)$$

Due to the statistical characterization of the reconstruction error by AMP, $\tilde{\mathbf{w}}_{k,0}$ and $\tilde{\mathbf{w}}_{k,1}$ are i.i.d. Gaussian. Now considering $\mathbf{h}$ as a deterministic channel, $U_{k,0}$ is a non-central chi-square distributed random variable and $U_{k,1}$ is a central chi-square distributed random variable, both with $N/2$ degrees of freedom. We can see that finding a closed-form expression of the probability of error involving these two distributions is complicated. On the other hand, as we are dealing with the reconstructed signal consisting of N Nyquist-rate samples, where given the nature of UWB signals, it is known that $N \longrightarrow \infty$, we can rightly consider both $U_{k,0}$ and $U_{k,1}$ as Gaussian distributed by using the central limit theorem. Now to find a closed-form expression of the BEP, let us proceed by defining the variable

$$\Delta^{\mathrm{recon}} \triangleq U_{k,0} - U_{k,1}. \quad (40)$$

Since $a_k = 0$ has been transmitted, the probability of error for the detector based on the reconstructed signal ($P_e^{(\mathrm{R-BEP})}$) can be defined as

$$P_e^{(\mathrm{R-BEP})} \triangleq P(\Delta^{\mathrm{recon}} < 0). \quad (41)$$

Since $U_{k,0}$ and $U_{k,1}$ are assumed to be Gaussian distributed, the decision variable Δ^{recon} can also be considered Gaussian distributed. We now proceed to find its mean and variance.

Since $\mathrm{E}\{\tilde{\mathbf{h}}^T \tilde{\mathbf{w}}_{k,0}\} = 0$, the mean of $U_{k,0}$ can be written as, $\mathrm{E}\{U_{k,0}\} = E_h + \mathrm{E}\{\|\tilde{\mathbf{w}}_{k,0}\|_2^2\}$ and the mean of $U_{k,1}$ is given by, $\mathrm{E}\{U_{k,1}\} = \mathrm{E}\{\|\tilde{\mathbf{w}}_{k,1}\|_2^2\}$. Now since $\|\tilde{\mathbf{w}}_{k,i}\|_2^2$ for $i = 0, 1$, is a chi-square distributed random variable, its variance is given by, $\mathrm{Var}\{\|\tilde{\mathbf{w}}_{k,i}\|_2^2\} = 2\frac{N}{2}\sigma_w^4$ where $\sigma_w^2 = \frac{\sigma^2}{\mu N_f} + \frac{1}{\mu N}\|\mathbf{u}_k - \hat{\mathbf{u}}_k\|_2^2$. We can further derive that, $\mathrm{Var}\{\tilde{\mathbf{h}}^T \tilde{\mathbf{w}}_{k,0}\} = \sigma_w^2 E_h$ where we use the fact $\mathrm{E}\{\tilde{\mathbf{w}}_{k,0}\tilde{\mathbf{w}}_{k,0}^T\} = \sigma_w^2 \mathbf{I}_{N/2}$. Therefore, we obtain, $\mathrm{Var}\{U_{k,0}\} = N\sigma_w^4 + 4\sigma_w^2 E_h$ and $\mathrm{Var}\{U_{k,1}\} = N\sigma_w^4$. Thus the mean of the variable Δ^{recon} is

$$\mathrm{E}\{\Delta^{\mathrm{recon}}\} = \mathrm{E}\{U_{k,0}\} - \mathrm{E}\{U_{k,1}\} = E_h \quad (42)$$

and its variance is

$$\begin{aligned} \mathrm{Var}\{\Delta^{\mathrm{recon}}\} &= \mathrm{Var}\{U_{k,0}\} + \mathrm{Var}\{U_{k,1}\} \\ &= 2N\sigma_w^4 + 4\sigma_w^2 E_h. \end{aligned} \quad (43)$$

The probability of error for the reconstructed signal can therefore be approximated by

$$\begin{aligned} P_e^{(\mathrm{R-BEP})} &= Q\left(\left[\frac{\mathrm{Var}\{\Delta^{\mathrm{recon}}\}}{(\mathrm{E}\{\Delta^{\mathrm{recon}}\})^2} \right]^{-\frac{1}{2}} \right) \\ &= Q\left(\left[4\frac{\sigma_w^2}{E_h} + 2N\left(\frac{\sigma_w^2}{E_h}\right)^2 \right]^{-\frac{1}{2}} \right) \end{aligned} \quad (44)$$

which is the instantaneous BEP of a deterministic channel. Finding an analytical expression for the average BEP of (44) is quite complicated. Therefore, the average BEP ($P_e^{(\mathrm{R-ABEP})}$)

can be approximated by numerically averaging $P_e^{(\mathrm{R-BEP})}$ over different channel realizations [44], i.e.,

$$P_e^{(\mathrm{R-ABEP})} = \frac{1}{N^{\mathrm{realiz}}} \sum_{i=0}^{N^{\mathrm{realiz}}-1} P_e^{(\mathrm{R-BEP})}(i) \qquad (45)$$

where $P_e^{(\mathrm{R-BEP})}(i)$ is the instantaneous BEP for the ith channel realization and N^{realiz} is the total number of channel realizations.

The analysis provided above is for the case when $\mathcal{M} = 2$. Exact BEP expressions for the case when $\mathcal{M} > 2$ are again difficult to derive. Nonetheless, an upper bound (that is a union bound) on the BEP of $\mathcal{M} - 1$ events can still be utilized [45], i.e.,

$$P_e^{(\mathrm{R-BEP})} \lessapprox \frac{\mathcal{M}}{2} Q\left(\left[4\frac{\sigma_w^2}{E_s} + 2N\left(\frac{\sigma_w^2}{E_s}\right)^2\right]^{-\frac{1}{2}}\right) \qquad (46)$$

where $E_s \triangleq E_h \log_2 \mathcal{M}$. The bound becomes tighter with increasing SNR and is exact for the case $\mathcal{M} = 2$.

B. Direct Compressed Detection

To derive the BEP expressions for the direct compressed detector, we consider an average compressed frame. Now given that $a_k = 0$ and $\mathcal{M} = 2$, the average compressed frame $\bar{\mathbf{y}}_k$ can be partitioned into two equal parts under Assumption 3: the signal part $\bar{\mathbf{y}}_{k,0}$ and the non-signal part $\bar{\mathbf{y}}_{k,1}$, i.e.,

$$\bar{\mathbf{y}}_{k,0} \triangleq [\bar{\mathbf{y}}_k]_{1:M/2} = \tilde{\mathbf{\Phi}}\tilde{\mathbf{h}} + \tilde{\bar{\boldsymbol{\xi}}}_{k,0} \qquad (47)$$

where $\tilde{\bar{\boldsymbol{\xi}}}_{k,0} \triangleq [\bar{\boldsymbol{\xi}}_k]_{1:M/2}$ and

$$\bar{\mathbf{y}}_{k,1} \triangleq [\bar{\mathbf{y}}_k]_{(M/2+1):M} = \tilde{\bar{\boldsymbol{\xi}}}_{k,1} \qquad (48)$$

where $\tilde{\bar{\boldsymbol{\xi}}}_{k,1} \triangleq [\bar{\boldsymbol{\xi}}_k]_{(M/2+1):M}$. We know that $\tilde{\bar{\boldsymbol{\xi}}}_{k,i}$ for $i = 0, 1$, is zero-mean with covariance matrix, $\mathrm{E}\{\tilde{\bar{\boldsymbol{\xi}}}_{k,i}\tilde{\bar{\boldsymbol{\xi}}}_{k,i}^T\} = \frac{\sigma^2}{\mu N_f}\mathbf{I}_{M/2}$ under Assumption 2. The energies corresponding to (47) and (48) can be defined as

$$Y_{k,0} \triangleq \|\bar{\mathbf{y}}_{k,0}\|_2^2 = E_{\tilde{h}} + 2\tilde{\mathbf{h}}^T\tilde{\mathbf{\Phi}}^T\tilde{\bar{\boldsymbol{\xi}}}_{k,0} + \|\tilde{\bar{\boldsymbol{\xi}}}_{k,0}\|_2^2 \qquad (49)$$

with $E_{\tilde{h}} = \|\tilde{\mathbf{\Phi}}\tilde{\mathbf{h}}\|_2^2$ and

$$Y_{k,1} \triangleq \|\bar{\mathbf{y}}_{k,1}\|_2^2 = \|\tilde{\bar{\boldsymbol{\xi}}}_{k,1}\|_2^2. \qquad (50)$$

Now the GML based energy detector for the compressed signal can be written as

$$Y_{k,0} \underset{1}{\overset{0}{\gtrless}} Y_{k,1} \qquad (51)$$

and the bit error probability for the compressed detector $P_e^{(\mathrm{C-BEP})}$ can be defined as

$$P_e^{(\mathrm{C-BEP})} \triangleq P(\Delta^{\mathrm{comp}} < 0) \qquad (52)$$

where

$$\Delta^{\mathrm{comp}} \triangleq Y_{0,0} - Y_{0,1}. \qquad (53)$$

Now, due to Assumption 2, $\tilde{\bar{\boldsymbol{\xi}}}_{k,i}$ is still zero-mean i.i.d. Gaussian. Therefore, by using the central limit theorem, both $Y_{0,0}$ and $Y_{0,1}$ can be assumed to be Gaussian distributed as $M \longrightarrow \infty$, which implies that Δ^{comp} is also a Gaussian distributed random variable. We can find an approximate closed-form expression for the probability of error by finding the mean and the variance of the variable Δ^{comp}.

Since $\mathrm{E}\{\tilde{\mathbf{h}}^T\tilde{\mathbf{\Phi}}^T\tilde{\bar{\boldsymbol{\xi}}}_{k,0}\} = 0$ and $\mathrm{E}\{\|\tilde{\bar{\boldsymbol{\xi}}}_{k,0}\|_2^2\} = \frac{M}{2}\frac{\sigma^2}{\mu N_f}$, the mean of $Y_{k,0}$ can be calculated as, $\mathrm{E}\{Y_{k,0}\} = E_{\tilde{h}} + \frac{M}{2}\frac{\sigma^2}{\mu N_f}$. Now, it can be proven that $\mathrm{Var}\{\tilde{\mathbf{h}}^T\tilde{\mathbf{\Phi}}^T\tilde{\bar{\boldsymbol{\xi}}}_{k,0}\} = \frac{\sigma^2}{\mu N_f}E_{\tilde{h}}$ and since $\|\tilde{\bar{\boldsymbol{\xi}}}_0\|_2^2$ is a chi-square distributed random variable with $M/2$ degrees of freedom, $\mathrm{Var}\{\|\tilde{\bar{\boldsymbol{\xi}}}_{k,0}\|_2^2\} = 2\frac{M}{2}\frac{\sigma^4}{\mu^2 N_f^2}$. Thus the variance of the decision variable $Y_{k,0}$ can be written as, $\mathrm{Var}\{Y_{k,0}\} = 4\frac{\sigma^2}{\mu N_f}E_{\tilde{h}} + M\frac{\sigma^4}{\mu^2 N_f^2}$. Similarly, it can be shown that the mean of $Y_{k,1}$, $\mathrm{E}\{Y_{k,1}\} = \frac{M}{2}\frac{\sigma^2}{\mu N_f}$ and its variance, $\mathrm{Var}\{Y_{k,1}\} = M\frac{\sigma^4}{\mu^2 N_f^2}$. Thus the mean of the variable Δ^{comp} is

$$\mathrm{E}\{\Delta^{\mathrm{comp}}\} = \mathrm{E}\{Y_{k,0}\} - \mathrm{E}\{Y_{k,1}\} = E_{\tilde{h}} \qquad (54)$$

and its variance is

$$\begin{aligned}\mathrm{Var}\{\Delta^{\mathrm{comp}}\} &= \mathrm{Var}\{Y_{k,0}\} + \mathrm{Var}\{Y_{k,1}\} \\ &= 4\frac{\sigma^2}{\mu N_f}E_{\tilde{h}} + 2M\frac{\sigma^4}{\mu^2 N_f^2}. \end{aligned} \qquad (55)$$

Since Δ^{comp} is a Gaussian distributed random variable, the approximate closed-form expression for the probability of error can be derived as

$$P_e^{(\mathrm{C-BEP})} = Q\left(\left[4\frac{\sigma^2/\mu}{N_f E_{\tilde{h}}} + 2M\left(\frac{\sigma^2/\mu}{N_f E_{\tilde{h}}}\right)^2\right]^{-\frac{1}{2}}\right). \qquad (56)$$

Note that (56) leads to the probability of error of the Nyquist-rate sampled received signal if M is replaced by N and $\mu = 1$. It is given by

$$P_e^{(\mathrm{N-BEP})} = Q\left(\left[4\frac{\sigma^2}{N_f E_h} + 2N\left(\frac{\sigma^2}{N_f E_h}\right)^2\right]^{-\frac{1}{2}}\right). \qquad (57)$$

We can see that (56) and (57) are expressions for the instantaneous BEP. Average BEP results can again be found by numerical averaging over different channel realizations as in (45).

V. CS Based Detection for a Gaussian Distributed Channel

In this section, we derive the BEP expressions for the proposed CS based detectors when the channel is Gaussian distributed. We assume that the channel elements are zero-mean i.i.d. Gaussian, i.e., $h_i \sim \mathcal{N}(0, 1)$. For the ease of the derivations, we further assume that the channel spread $T_h = T_{\mathcal{M}}$ and thus, $L = N_{\mathcal{M}}$. The Gaussian assumption on the channel may not be realistic but it helps to provide some intuition regarding

the influence of the channel on the average BEP. Here again, we consider $\mathcal{M} = 2$ and $a_k = 0$.

A. Reconstruction Based Detection

In this section, we look at the reconstruction based detector when the channel is Gaussian distributed and derive a closed-form expression of its theoretical BEP. Thus, in the context of (34), under Assumption 1 we can say from (38) and (39) that $\breve{\mathbf{u}}_{k,0} \sim \mathcal{N}(\mathbf{0}, (1+\sigma_w^2)\mathbf{I}_{N/2})$ and $\breve{\mathbf{u}}_{k,1} \sim \mathcal{N}(\mathbf{0}, \sigma_w^2\mathbf{I}_{N/2})$. From (35) and (36), this means that $U_{k,0}$ and $U_{k,1}$, both being the sum of Gaussian distributed random variables are chi-square distributed with $N/2$ degrees of freedom. The pdf of $U_{k,0}$ is given by [45]

$$p_{U_{k,0}}(u_{k,0}) = \frac{{u_{k,0}}^{\frac{N}{4}-1}}{\sigma_r^{\frac{N}{2}} 2^{\frac{N}{4}} \Gamma\left(\frac{N}{4}\right)} e^{\frac{-u_{k,0}}{2\sigma_r^2}}$$

where $\sigma_r^2 \triangleq 1+\sigma_w^2$, and the pdf of $U_{k,1}$ is given by [45]

$$p_{U_{k,1}}(u_{k,1}) = \frac{u_{k,1}^{\frac{N}{4}-1}}{\sigma_w^{\frac{N}{2}} 2^{\frac{N}{4}} \Gamma\left(\frac{N}{4}\right)} e^{\frac{-u_{k,1}}{2\sigma_w^2}}.$$

Now from (37) the average BEP for the reconstruction based detector (R-ABEP), given a zero symbol is transmitted is

$$P_e^{(\mathrm{R-ABEP})} = P(U_{k,0} < U_{k,1} | a_k = 0). \tag{58}$$

The probability of a correct decision given that a zero is transmitted can then be written as

$$\begin{aligned}\bar{P}_c &= P(U_{k,1} < U_{k,0} | a_k = 0) \\ &= \int_0^{u_{k,0}} p_{U_{k,1}}(u_{k,1})\, du_{k,1}\end{aligned}$$

which can be simplified to

$$\bar{P}_c = \frac{\gamma\left(\frac{N}{4}, \frac{u_{k,0}}{2\sigma_w^2}\right)}{\Gamma\left(\frac{N}{4}\right)}$$

where $\gamma(\cdot,\cdot)$ is the lower-incomplete-gamma function and $\Gamma(\,\cdot\,)$ is the gamma function such that $\gamma(n,u) = \int_0^u t^{n-1}e^{-t}\,dt$ and $\Gamma(n) = \int_0^\infty t^{n-1}e^{-t}\,dt$, [46]. The average BEP is therefore given by

$$\begin{aligned}P_e^{(\mathrm{R-ABEP})} &= 1 - \int_0^\infty \bar{P}_c\, p_{U_{k,0}}(u_{k,0})\, du_{k,0} \\ &= 1 - \int_0^\infty \frac{\gamma\left(\frac{N}{4}, \frac{u_{k,0}}{2\sigma_w^2}\right)}{\Gamma\left(\frac{N}{4}\right)} \frac{{u_{k,0}}^{\frac{N}{4}-1}}{\sigma_r^{\frac{N}{2}} 2^{\frac{N}{4}} \Gamma\left(\frac{N}{4}\right)} e^{\frac{-u_{k,0}}{2\sigma_r^2}}\, du_{k,0}.\end{aligned} \tag{59}$$

By using ([46], (6.455.2)), we can reduce (59) to the following closed-form expression

$$\begin{aligned}P_e^{(\mathrm{R-ABEP})} = 1 - \frac{2\Gamma\left(\frac{N}{2}\right)}{\frac{N}{2}\left[\Gamma\left(\frac{N}{4}\right)\right]^2} \left[\frac{\sigma_r\sigma_w}{\sigma_r^2+\sigma_w^2}\right]^{\frac{N}{2}} \\ \times {}_2F_1\left(1, \frac{N}{2}; \frac{N}{4}+1; \frac{\sigma_r^2}{\sigma_r^2+\sigma_w^2}\right),\end{aligned} \tag{60}$$

where ${}_2F_1(\cdot,\cdot;\cdot;\cdot)$ is the Gaussian hypergeometric function defined by ([46], (9.14.2)). Hence, we have obtained a closed-form expression for the average BEP of the reconstruction based energy detector for a channel with i.i.d. zero-mean Gaussian elements.

B. Direct Compressed Detection

In this section, we present the BEP expressions for the detector based on the compressed signals when the channel is Gaussian distributed. From (47), we can see that since $\tilde{\mathbf{h}}$ is Gaussian, $\tilde{\mathbf{\Phi}}\tilde{\mathbf{h}}$ will also be Gaussian with covariance matrix $\mathrm{E}\{(\tilde{\mathbf{\Phi}}\tilde{\mathbf{h}})(\tilde{\mathbf{\Phi}}\tilde{\mathbf{h}})^T\} = \frac{1}{\mu}\mathbf{I}_{M/2}$ under Assumptions 2 and 3. Consequently, $\bar{\mathbf{y}}_{k,0}$ will be zero-mean Gaussian distributed with covariance matrix $\mathrm{E}\{\bar{\mathbf{y}}_{k,0}\bar{\mathbf{y}}_{k,0}^T\} = \frac{1}{\mu}(1+\frac{\sigma^2}{N_f})\mathbf{I}_{M/2}$. Thus we can write $\bar{\mathbf{y}}_{k,0} \sim \mathcal{N}(\mathbf{0}, \sigma_c^2\mathbf{I}_{M/2})$, where $\sigma_c^2 \triangleq \frac{1}{\mu}(1+\frac{\sigma^2}{N_f})$ and from (48) we can write $\bar{\mathbf{y}}_{k,1} \sim \mathcal{N}(\mathbf{0}, \sigma_f^2\mathbf{I}_{M/2})$, where $\sigma_f^2 \triangleq \frac{\sigma^2}{\mu N_f}$. Therefore, from (49) and (50), we can say that $Y_{k,0}$ and $Y_{k,1}$ are chi-square distributed random variables, both with $M/2$ degrees of freedom.

Now from (51), we can observe that the average BEP for the compressed detector (C-ABEP), given a zero transmitted-symbol

$$P_e^{(\mathrm{C-ABEP})} = P(Y_{k,0} < Y_{k,1} | a_k = 0). \tag{61}$$

The probability of a correct decision given that a zero is transmitted can then be written as

$$\begin{aligned}\bar{P}_c &= P(Y_{k,1} < Y_{k,0} | a_k = 0) \\ &= \int_0^{y_{k,0}} p_{Y_{k,1}}(y_{k,1})\, dy_{k,1} \\ &= \int_0^{y_{k,0}} \frac{y_{k,1}^{\frac{M}{4}-1}}{\sigma_f^{\frac{M}{2}} 2^{\frac{M}{4}} \Gamma\left(\frac{M}{4}\right)} e^{\frac{-y_{k,1}}{2\sigma_f^2}}\, dy_{k,1},\end{aligned}$$

which can be simplified to

$$\bar{P}_c = \frac{\gamma\left(\frac{M}{4}, \frac{y_{k,0}}{2\sigma_f^2}\right)}{\Gamma\left(\frac{M}{4}\right)}.$$

The average BEP is then given by

$$\begin{aligned}P_e^{(\mathrm{C-ABEP})} &= 1 - \int_0^\infty \bar{P}_c\, p_{Y_{k,0}}(y_{k,0})\, dy_{k,0} \\ &= 1 - \int_0^\infty \frac{\gamma\left(\frac{M}{4}, \frac{y_{k,0}}{2\sigma_f^2}\right)}{\Gamma\left(\frac{M}{4}\right)} \frac{{y_{k,0}}^{\frac{M}{4}-1}}{\sigma_c^{\frac{M}{2}} 2^{\frac{M}{4}} \Gamma\left(\frac{M}{4}\right)} e^{\frac{-y_{k,0}}{2\sigma_c^2}}\, dy_{k,0}.\end{aligned} \tag{62}$$

By using ([46], (6.455.2)), we can reduce (62) to

$$\begin{aligned}P_e^{(\mathrm{C-ABEP})} = 1 - \frac{2\Gamma\left(\frac{M}{2}\right)}{\frac{M}{2}\left[\Gamma\left(\frac{M}{4}\right)\right]^2} \left[\frac{\sigma_c\sigma}{\sigma_c^2+\sigma_f^2}\right]^{\frac{M}{2}} \\ \times {}_2F_1\left(1, \frac{M}{2}; \frac{M}{4}+1; \frac{\sigma_c^2}{\sigma_c^2+\sigma_f^2}\right)\end{aligned} \tag{63}$$

which is the closed-form expression for the average BEP of the optimal compressed energy detector for a channel with i.i.d. zero-mean Gaussian elements. Now from (63), the average BEP of the ED for the Nyquist-rate sampled received signal (N-ABEP) can be written as [47]

$$P_e^{(\mathrm{N-ABEP})} = 1 - \frac{2\Gamma\left(\frac{N}{2}\right)}{\frac{N}{2}\left[\Gamma\left(\frac{N}{4}\right)\right]^2}\left[\frac{\sigma_{c0}\sigma_{f0}}{\sigma_{c0}^2+\sigma_{f0}^2}\right]^{\frac{N}{2}} \times {}_2F_1\left(1, \frac{N}{2}; \frac{N}{4}+1; \frac{\sigma_{c0}^2}{\sigma_{c0}^2+\sigma_{f0}^2}\right) \quad (64)$$

where $\sigma_{c0}^2 \triangleq (1+\frac{\sigma^2}{N_f})$ and $\sigma_{f0}^2 \triangleq \frac{\sigma^2}{N_f}$.

VI. Simulations

In this section, we present some simulation results for the different detectors developed in the previous sections for the binary PPM communications scenario. We provide two groups of simulations. One where we consider a deterministic channel and the other where we assume the channel to be Gaussian distributed. For the measurement matrices, Assumption 3 holds true in general. Further, we consider a measurement matrix whose elements are random Gaussian under Assumption 1 as well as a measurement matrix whose rows have been orthogonalized under Assumption 2.

For the reconstruction of the signal, AMP suggests an optimal thresholding policy in the form of the relationship $\lambda^{[n]} = \tau\sigma_w^{[n]}$ at the nth iteration, but it requires the knowledge of the original signal and therefore, it is not practically feasible. For our purpose, we use the following alternative relationship as suggested in [38]

$$\lambda^{[n]} = \lambda + \frac{1}{\mu}\lambda^{[n-1]}\left\langle \mathcal{S}'\left(\hat{\mathbf{u}}_k^{[n-1]} + \mathbf{\Phi}^T\mathbf{z}_k^{[n-1]}, \lambda^{[n-1]}\right)\right\rangle \quad (65)$$

where λ is a constant. Thus the threshold value keeps developing for every AMP iteration. Further, for the BEP expression of the spreading-factor dependent energy detector (26), we use the following expression from [12]

$$P_e^{(\mathrm{SN-BEP})} = Q\left(\left[4\frac{\sigma^2}{N_f E_h} + 4LN_f\left(\frac{\sigma^2}{N_f E_h}\right)^2\right]^{-\frac{1}{2}}\right) \quad (66)$$

and the corresponding average BEP ($P_e^{(\mathrm{SN-ABEP})}$) is obtained by averaging (66) over the channel realizations as in (45).

For Figs. 4 to 8, we consider the IEEE 802.15.3a CM1 (line-of-sight) channel model [11]. The channel parameters are chosen as follows: the cluster arrival rate $\Lambda_{\mathrm{ch}} = 0.0233$ nsec^{-1}, the ray arrival rate within a cluster $\lambda_{\mathrm{ch}} = 2.5$ nsec^{-1}, the cluster decay factor $\Gamma_{\mathrm{ch}} = 2.5$ and the ray decay factor within a cluster $\gamma_{\mathrm{ch}} = 4.3$. The transmitted pulse waveform $q(t)$ is the second derivative of a Gaussian pulse of unit energy with pulse duration $T_q = 1$ nsec. In general, the frame length is taken as $T_f = 150$ nsec and a receive filter bandwidth of 3 GHz is considered. Thus each frame has $N = 900$ Nyquist-rate samples.

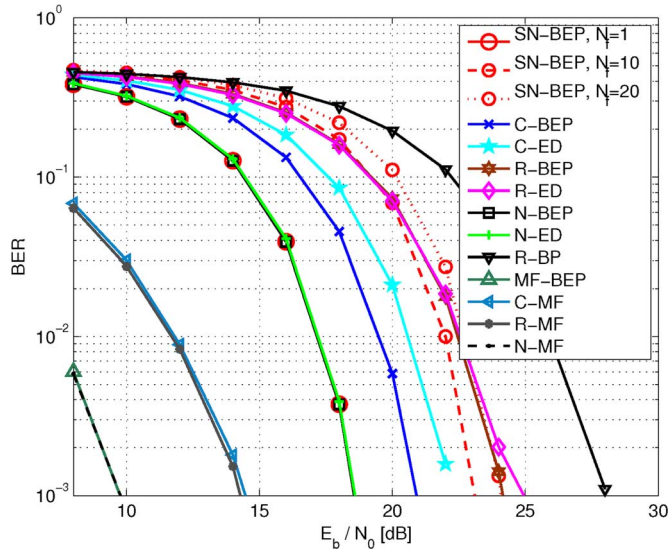

Fig. 4. Comparison of different detectors with random measurement matrix and a deterministic channel.

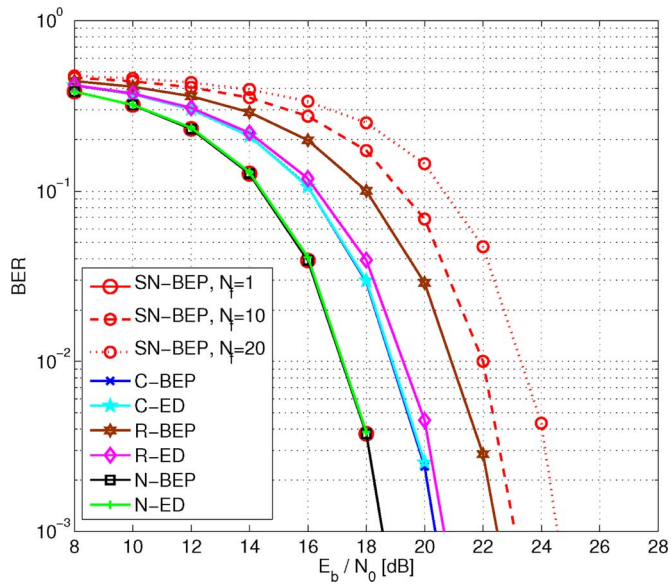

Fig. 5. Comparison of different detectors with orthogonal measurement matrix and a deterministic channel.

Fig. 4 shows the instantaneous BER results for different detectors, i.e., C-ED, R-ED and N-ED, along with some theoretical BEP plots, i.e., SN-BEP, C-BEP, R-BEP and N-BEP, with a Gaussian distributed random measurement matrix (Assumption 1). Here, we consider signal transmission with a varying number of frames per symbol, i.e., $N_f = 1, 10, 20$. We can see that with increasing spreading factor, the SN-BEP keeps decreasing. Whereas the BEP results for the detectors with optimal frame combining remain consistent and do not vary with a varying number of frames. The performance of the R-ED follows the theoretical expression R-BEP exactly. The C-ED remains a bit away from the C-BEP because the Gaussian measurement matrix does not guarantee (5). Now with regard to the performance of the compressed detectors against the Nyquist-rate detectors,

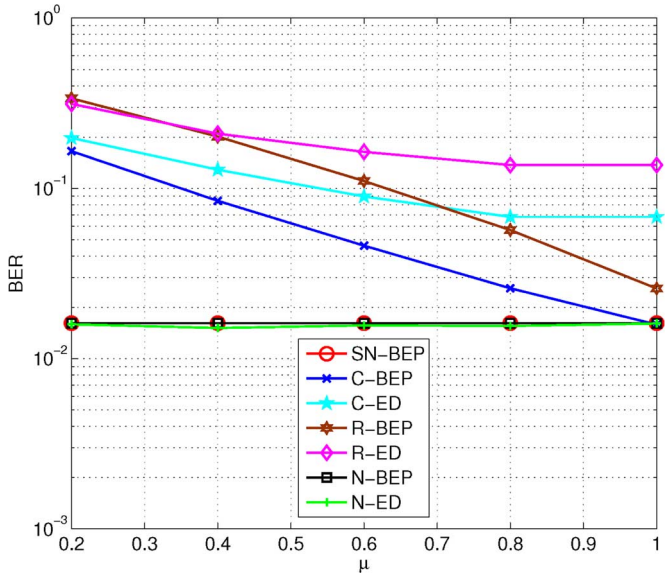

Fig. 6. Comparison of detectors for varying compression ratio with random measurement matrix and a deterministic channel.

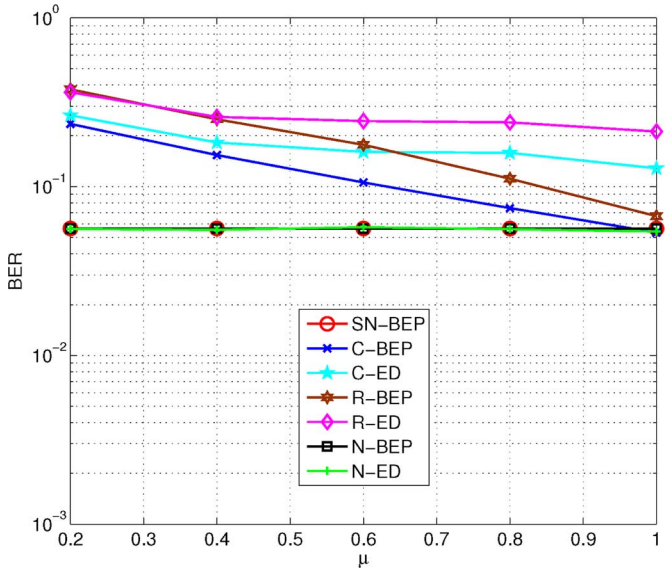

Fig. 7. Comparison of detectors for varying compression ratio with random measurement matrix and a deterministic channel.

we see that at a compression ratio of $\mu = 0.5$, i.e., the sampling rate is only 50% of the Nyquist-rate, the compressed rate detectors offer a reasonably good performance (see [48] for details on the loss incurred due to CS). The C-ED performs better than the reconstructed version, i.e., the R-ED. The reason is that the reconstruction process loses some information whereas the compressed domain detection preserves the signal information albeit in a compressed form and gives a better performance. The difference between N-BEP and C-BEP is around 2 to 3 dB at a BER of 10^{-3}. Thus CS based EDs are a viable option. For the sake of comparison, we also include in this figure the performance of matched filter (MF) based compressed detectors (where it is assumed that the channel is known); when detection is carried out on the reconstructed signal (R-MF) and when it is carried out on the compressed signal directly (C-MF), along

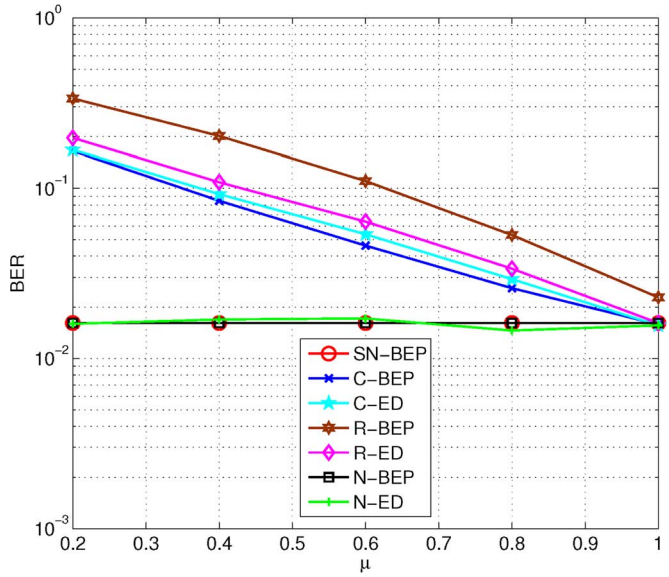

Fig. 8. Comparison of detectors for varying compression ratio with orthogonal measurement matrix and a deterministic channel.

with the MF for the Nyquist-rate sampled signal (N-MF) and its theoretical plot (MF-BEP).

Fig. 5 shows the instantaneous BER performance for different detectors when the measurement matrix has orthogonal rows (Assumption 2). Here $\mu = 0.5$ and $N_f = 1, 10, 20$. We see that the performance of C-ED has improved and it falls exactly on the C-BEP curve. R-ED does not coincide with R-BEP because the expression for the R-BEP is based on a random measurement matrix under Assumption 1, but its performance has also improved in comparison to the previous figure. The SN-BEP keeps again worsening with an increasing value of N_f.

Fig. 6 shows a BER comparison of different detectors with varying compression ratios when the measurement matrix is Gaussian distributed (Assumption 1). We fix the SNR at 17 dB. Here we see that the performance of the R-ED and C-ED saturates after a certain compression ratio. The reason is that if N is not very large then as the number of measurements increases, the probability of having correlations within the measured values increases as well (see (6)). In Fig. 7, we increase the frame time to $T_f = 300$ nsec. We can see that although the overall performance of all the detectors has been scaled, nonetheless R-ED and the C-ED show a tendancy of improvement for the larger value of N.

Fig. 8 shows a BER comparison of different detectors with varying values of μ when the orthogonal measurement matrix is used (Assumption 2). We consider here an SNR of 17 dB. We can see that the performance of both the R-ED and C-ED has improved and does not saturate with increasing μ. C-ED follows C-BEP exactly but R-ED remains away from R-BEP because of the absence of a random measurement matrix.

From Figs. 9 to 12, we consider a Gaussain distributed multipath channel, i.e., the channel samples are zero-mean, unit-variance Gaussian. Considering the limitations of the simulation software, i.e., Matlab, viz a viz (60), (63) and (64), we take a frame length of $T_f = 100$ nsec and a receive filter bandwidth

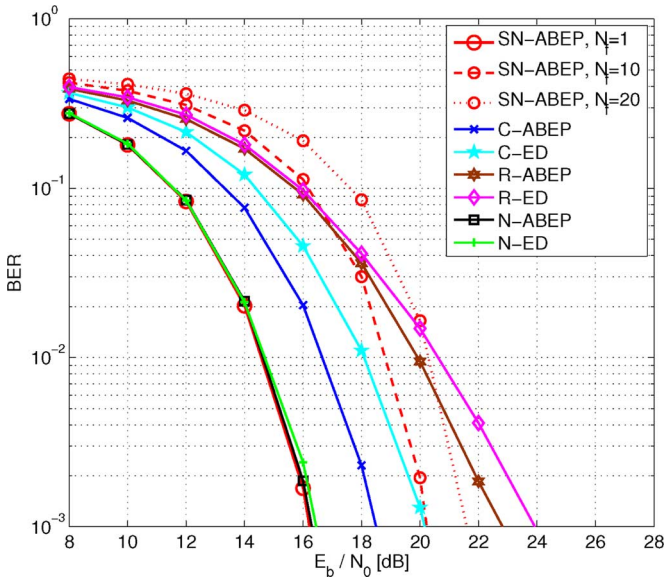

Fig. 9. Comparison of different detectors with random measurement matrix and Gaussian channel.

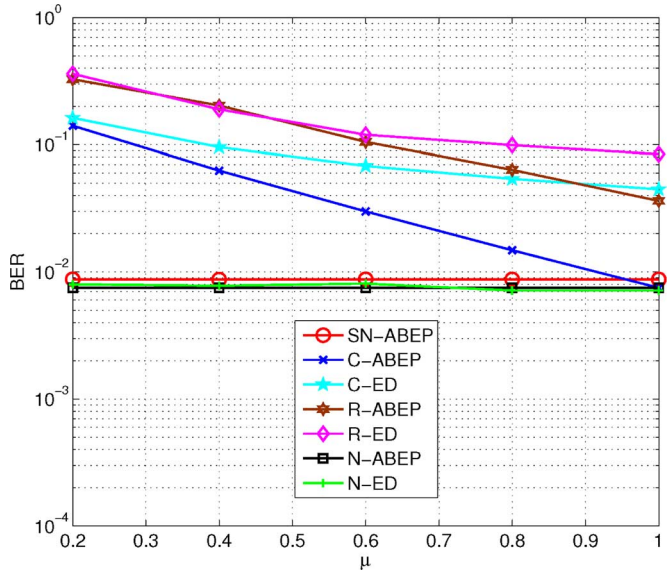

Fig. 11. Comparison of detectors for varying compression ratio with random measurement matrix and Gaussian channel.

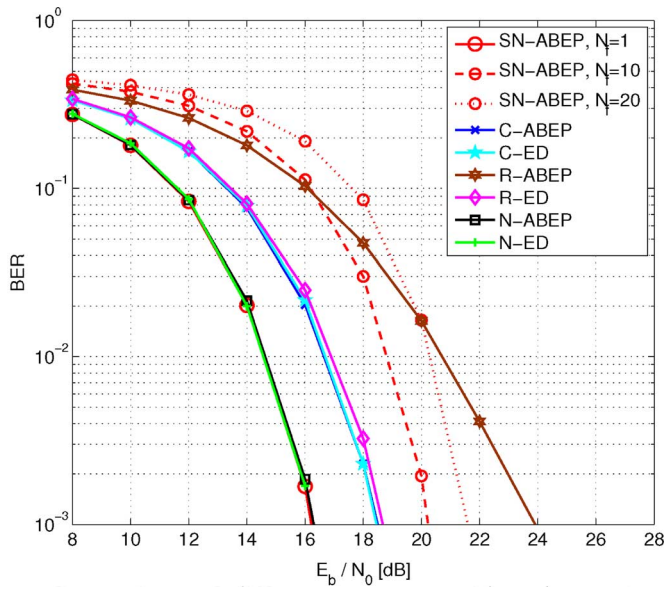

Fig. 10. Comparison of different detectors with orthogonal measurement matrix and Gaussian channel.

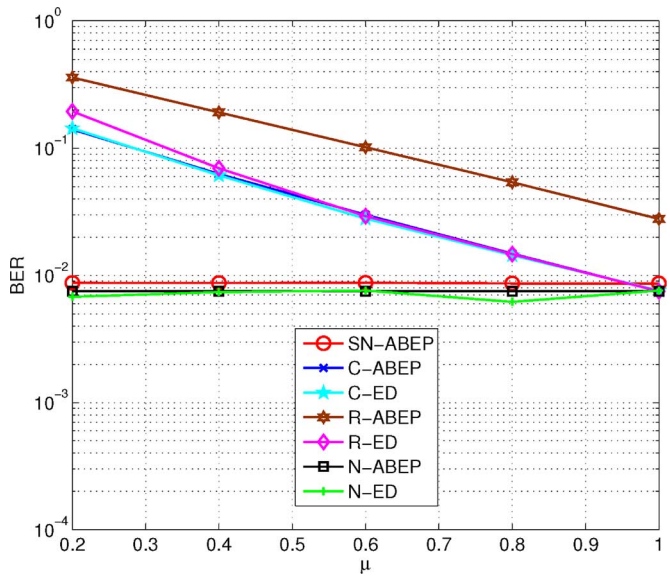

Fig. 12. Comparison of detectors for varying compression ratio with orthogonal measurement matrix and Gaussian channel.

of $B = 1$ GHz. Now every frame has $N = 200$ Nyquist-rate samples.

Fig. 9 shows the average BER results for C-ED, R-ED and N-ED along with the theoretical BEPs i.e., SN-ABEP, C-ABEP, R-ABEP and N-ABEP, with a Gaussian distributed channel. SN-ABEP has been obtained by averaging the SN-BEP results over all channel realizations. We consider a random measurement matrix (Assumption 1) with the compression ratio $\mu = 0.5$ and $N_f = 1, 10, 20$. The simulation results for the detectors follow the BEP expressions quite closely. We can see that the suboptimal detector SN-ABEP, once again falls a prey to the increasing spreading factor and its performance keeps decreasing. The proposed detectors remain unaffected by this factor. The R-ED follows the R-ABEP exactly but C-ED is a bit away from C-ABEP due to the randomness of the measurement matrix.

Fig. 10 shows the average BER comparison of different detectors when an orthogonal measurement matrix is used (Assumption 2). Here again $\mu = 0.5$ and $N_f = 1, 10, 20$. We see that R-ED is away from R-ABEP but C-ED follows C-ABEP exactly due to the choice of the measurement matrix. In general the performance of the proposed CS based energy detectors, C-ED and R-ED, remains reasonable in comparison to the Nyquist-rate based energy detector, N-ED.

Figs. 11 and 12 show the average BER results for the presented detectors against a varying compression ratio at an SNR of 15 dB, for a random and an orthogonal measurement matrix, respectively. The number of frames per symbol is $N_f = 1$. We

TABLE I
SUMMARY OF THE PROPOSED DETECTORS

Features	R-ED	C-ED
Sample Form	Reconstructed samples	Compressed samples
Theoretical BEP	Requires random $\mathbf{\Phi}$	Requires orthogonal $\mathbf{\Phi}$
Timing Information	Can be relaxed	Required
$\tilde{\mathbf{\Phi}}$ (over $T_{\mathcal{M}}$)	Independent	Must be identical

can see that with an increasing compression ratio the performance of the proposed detectors increases.

Discussion

From the above simulation results, we can see that C-ED performs better than R-ED in terms of BER. Therefore, a question arises as to what is the need of R-ED at all. First, it should be noted that despite a better performance, C-ED works under stringent constraints of exact synchronization. If full timing information is not available, the performance of C-ED will deteriorate. On the other hand, such constraints can be relaxed with respect to R-ED. Since R-ED has to reconstruct the received signal from its compressed samples as an initial step, the timing information can be extracted from the reconstructed signal by resorting to existing methods proposed for Nyquist-rate sampled signals. Secondly, note that the measurement process used in the paper is assumed to be identical (which usually will be the case) for each pulse position (i.e., over $T_{\mathcal{M}}$). If this process is changed either due to perturbations or on purpose, the performance of C-ED will be severely affected. On the other hand, the performance of R-ED is robust to changing measurement process. Thus, we can say that both proposed detectors are important and have their own merits. Table I provides a summary of the salient features of our proposed detectors.

Further, we would like to comment on the issue of narrow band interference (NBI) in UWB signals w.r.t. our proposed detectors. NBI has been one of the major challenges as it reduces the dynamic range and necessitates more resolution bits for the effective detection of UWB signals [49], [50], causing an increase in ADC power consumption [5]. In this regard, the method presented in [22] to handle NBI can be easily incorporated in our proposed detection schemes. If the measurement matrix is designed as a Fourier ensemble with frequencies uniformly spaced over the signal bandwidth, then NBI can be identified by taking the square of the measurements. The measurements affected by NBI will have the highest magnitudes. The block of such contaminated measurements can be discarded and detection can be carried out on the rest of the measurements. Thus by adopting this idea, our proposed detectors can be robust against NBI as well.

VII. CONCLUSION

In this paper we have developed compressive sampling based energy detectors to reduce the sampling rate much below the Nyquist rate. We have shown that compressive sampling helps in the realization of spreading-factor independent energy detectors. Our energy detectors work both on the reconstructed signal as well as on the compressed signal directly without reconstruction. We have derived theoretical BEP expressions to guage the performance of compressive sampling based energy detectors which can also be extended to Nyquist-rate sampling based energy detectors. Simulation results prove the validity of these expressions if the choice of measurement matrix follows the assumptions adopted in the theoretical derivations.

REFERENCES

[1] M. Ghavami, L. B. Michael, and R. Kohno, *Ultra Wideband Signals and Systems in Communication Engineering*, 2nd ed. New York, NY, USA: Wiley, 2007.

[2] M. Z. Win and R. A. Scholtz, "Impulse radio: How it works," *IEEE Commun. Lett.*, vol. 2, no. 2, pp. 36–38, Feb. 1998.

[3] M. Vetterli, P. Marziliano, and T. Blu, "Sampling signals with finite rate of innovation," *IEEE Trans. Signal Process.*, vol. 50, no. 6, pp. 1417–1428, Jun. 2002.

[4] M. Unser, "Sampling-50 years after Shannon," *Proc. IEEE*, vol. 88, no. 4, pp. 569–587, Apr. 2000.

[5] B. Le, T. Rondeau, J. Reed, and C. Bostian, "Analog-to-digital converters," *IEEE Signal Process. Mag.*, vol. 22, no. 6, pp. 69–77, Nov. 2005.

[6] R. Walden, "Analog-to-digital converter survey and analysis," *IEEE J. Sel. Areas Commun.*, vol. 17, no. 4, pp. 539–550, Apr. 1999.

[7] S. Kirolos, J. Laska, M. Wakin, M. Duarte, D. Baron, T. Ragheb, Y. Massoud, and R. Baraniuk, "Analog-to-information conversion via random demodulation," presented at the IEEE Dallas Circuits and Systems Workshop (DCAS), Dallas, TX, USA, 2006.

[8] T. Blu, P. L. Dragotti, M. Vetterli, P. Marziliano, and L. Coulot, "Sparse sampling of signal innovations," *IEEE Signal Process. Mag.*, pp. 31–40, Mar. 2008.

[9] D. L. Donoho, "Compressed sensing," *IEEE Trans. Inf. Theory*, vol. 52, no. 4, pp. 1289–1306, Apr. 2006.

[10] E. Candès, J. Romberg, and T. Tao, "Robust Uncertainty Principles: Exact signal reconstruction from highly incomplete frequency information," *IEEE Trans. Inf. Theroy*, vol. 52, no. 2, pp. 489–509, Feb. 2006.

[11] A. F. Molisch, J. R. Foerster, and M. Pendergrass, "Channel models for ultrawideband personal area networks," *IEEE Wireless Commun.*, vol. 10, no. 6, pp. 14–21, Dec. 2003.

[12] C. Carbonelli and U. Mengali, "M-PPM noncoherent receivers for UWB applications," *IEEE Trans. Wireless Commun.*, vol. 5, no. 8, pp. 2285–2294, Aug. 2006.

[13] S. Dubouloz, B. Denis, S. de Rivaz, and L. Ouvry, "Performance analysis of LDR UWB non-coherent receivers in multipath environments," in *Proc. IEEE Int. Conf. Ultra-Wideband*, Sep. 2005.

[14] Y. Souilmi and R. Knopp, "On the achievable rates of ultra-wideband PPM with non-coherent detection in multipath environments," in *Proc. IEEE Int. Conf. Commun.*, May 2003, vol. 5, pp. 3530–3534.

[15] Y. Vanderperren, G. Leus, and W. Dehaene, "Performance analysis of a flexible subsampling receiver for pulsed UWB signals," *IEEE Trans. Wireless Commun.*, vol. 8, no. 8, pp. 4134–4142, Aug. 2009.

[16] J. Kusuma, A. Ridolfi, and M. Vetterli, "Sampling of communication systems with bandwidth expansion," in *Proc. IEEE Int. Commun. Conf. (ICC)*, May 2002.

[17] J. Kusuma, I. Maravic, and M. Vetterli, "Sampling with finite rate of innovation: Channel and timing estimation for UWB and GPS," in *Proc. IEEE Int. Commun. Conf. (ICC)*, May 2003.

[18] Z. Wang, G. R. Arce, J. L. Paredes, and B. M. Sadler, "Compressed detection for ultra-wideband impulse radio," in *Proc. IEEE Signal Process. Adv. Wireless Commun. (SPAWC)*, 2007.

[19] Z. Wang, G. R. Arce, B. M. Sadler, J. L. Paredes, and X. Ma, "Compressed detection for pilot assisted ultra-wideband impulse radio," in *Proc. IEEE Int. Conf. Ultra-Wideband (ICUWB)*, 2007.

[20] A. Oka and L. Lampe, "A compressed sensing receiver for UWB impulse radio in bursty applications like wireless sensor networks," *Phys. Commun.*, vol. 2, no. 4, pp. 248–264, Dec. 2009.

[21] Z. Wang, G. R. Arce, B. M. Sadler, J. L. Pardes, S. Hoyos, and Z. Yu, "Compressed UWB signal detection with narrowband interference mitigation," in *Proc. IEEE Int. Conf. Ultra-Wideband (ICUWB)*, 2008.

[22] A. Oka and L. Lampe, "Compressed sensing reception of bursty UWB impulse radio is robust to narrow-band interference," in *IEEE Global Commun. Conf. (IEEE GLOBECOM)*, 2009.

[23] J. Paredes, G. R. Arce, and Z. Wang, "Ultra-wideband compressed sensing: Channel estimation," *IEEE J. Sel. Topics Signal Process.*, vol. 1, pp. 383–395, Oct. 2007.

[24] P. Zhang, Z. Hu, R. C. Qiu, and B. M. Sadler, "A compressed sensing based ultra-wideband communication system," in *Proc. IEEE Int. Commun. Conf. (ICC)*, 2009.
[25] K. Gedalyahu and Y. C. Eldar, "Time-delay estimation from low-rate samples: A union of subspaces approach," *IEEE Trans. Signal Process.*, vol. 58, no. 6, pp. 3017–3031, Jun. 2010.
[26] S. Gishkori, G. Leus, and V. Lottici, "Compressive sampling based differential detection for UWB impulse radio signals," *Elsevier Phys. Commun.*, vol. 5, no. 2, Jun. 2012.
[27] M. A. Davenport, P. T. Boufounos, M. B. Wakin, and R. G. Baraniuk, "Signal processing with compressive measurements," *IEEE J. Sel. Topics Signal Process.*, vol. 4, no. 2, pp. 445–460, Apr. 2010.
[28] "Revision of Part 15 of the commissions rules regarding ultra-wideband transmission systems," ET Docket 98-153, FCC Tech. Rep., 2002.
[29] T. Ragheb, J. Laska, H. Nejati, S. Kirolos, R. Baraniuk, and Y. Massoud, "A prototype hardware for random demodulation based compressive analog-to-digital conversion," in *Proc. Int. Midwest Symp. Circuits Syst. (MWSCAS) 2008*, Aug. 2008, pp. 37–40.
[30] Z. Yu and S. Hoyos, "Mixed-signal parallel compressed sensing and reception for cognitive radio," in *Proc. IEEE Int. Conf. Acoust., Speech, Signal Process. (ICASSP)*, 2008.
[31] S. S. Chen, D. L. Donoho, and M. A. Saunders, "Atomic decomposition by basis pursuit," *SIAM J. Sci. Comput.*, vol. 43, no. 1, pp. 129–159, 2001.
[32] Y. C. Pati, R. Rezaiifar, and P. S. Krishnaprasad, "Orthogonal matching pursuit: Recursive function approximation with applicants to wavelet decomposition," in *Proc. 27th Annu. Asilomar Conf. Signals, Syst., Comput.*, Nov. 1993, vol. 1, pp. 40–44.
[33] J. A. Tropp and A. C. Gilbert, "Signal recovery from random measurements via orthogonal matching pursuit," *IEEE Trans. Inf. Theory*, vol. 53, no. 12, pp. 4655–4666, Dec. 2007.
[34] D. Needell and J. A. Tropp, "COSAMP: Iterative signal recovery from incomplete and inaccurate samples," *Commun. ACM*, vol. 53, no. 12, pp. 93–100, Dec. 2010.
[35] A. Maleki and D. L. Donoho, "Optimally tuned iterative reconstruction algorithms for compressed sensing.," *IEEE J. Sel. Topics Signal Process.*, vol. 4, no. 2, pp. 330–341, Apr. 2010.
[36] D. L. Donoho, A. Maleki, and A. Montanari, "Message-passing algorithms for compressed sensing," in *Proc. Nat. Acad. Sci.*, 2009.
[37] D. L. Donoho, A. Maleki, and A. Montanari, "Message-passing algorithms for compressed sensing: I. Motivation and construction," in *Proc. IEEE Inf. Theory Workshop*, 2010.
[38] D. L. Donoho, A. Maleki, and A. Montanari, "Message-passing algorithms for compressed sensing: II. Analysis and validation," in *Proc. IEEE Inf. Theory Workshop*, 2010.
[39] J. Pearl, *Probablistic Reasoning in Intelligent Systems: Networks of Plausible Inference*. San Mateo, CA: Morgan Kaufmann, 1988.
[40] D. Baron, S. Sarvotham, and R. G. Baraniuk, "Bayesian compressive sensing via belief propagation," *IEEE Trans. Signal Process.*, vol. 58, no. 1, pp. 269–280, Jan. 2010.
[41] F. R. Kschischang, B. J. Frey, and H.-A. Loeliger, "Factor graphs and the sum-product algorithm," *IEEE Trans. Inf. Theory*, vol. 47, no. 2, pp. 498–519, Feb. 2001.
[42] M. Bayati and A. Montanari, "The dynamics of message passing on dense graphs, with applications to compressed sensing," *IEEE Trans. on Information Theory*, vol. 57, no. 2, pp. 764–785, Feb. 2011.
[43] S. Gishkori, G. Leus, and H. Deliç, "Energy detection of wideband and ultra-wideband PPM," in *Proc. IEEE Global Commun. (IEEE GLOBECOM)*, Dec. 2010.
[44] J. D. Choi and W. E. Stark, "Performance of ultra-wideband communications with suboptimal receivers in multipath channels," *IEEE J. Sel. Areas Commun.*, vol. 20, no. 9, pp. 1754–1766, Dec. 2002.
[45] J. G. Proakis, *Digital Communications*, 4th ed. New York, NY, USA: McGraw-Hill, 2001.
[46] I. S. Gradshteyn and I. M. Ryzhik, *Table of Integrals, Series, and Products*, 6th ed. San Diego, CA, USA: Academic, 1996.
[47] S. Gishkori, G. Leus, and H. Deliç, "Energy detectors for sparse signals," in *Proc. IEEE Signal Process. Adv. Wireless Commun. (SPAWC)*, Jun. 2010.
[48] M. A. Davenport, J. N. Laska, J. R. Treichler, and R. G. Baraniuk, "The pros and cons of compressive sensing for wideband signal acquisition: Noise folding versus dynamic range," *IEEE Trans. Signal Process.*, vol. 60, no. 9, pp. 4628–4642, Sep. 2012.
[49] R. Harjani, J. Harvey, and R. Sainati, "Analog/RF physical layer issues for UWB systems," in *Proc. IEEE VLSI Design*, pp. 941–948.
[50] L. Lampe and K. Witrisal, "Challenges and recent advances in IR-UWB system design," in *Proc. IEEE Int. Symp. Circuits and Syste. (ISCAS)*, pp. 3288–3291.

Shahzad Gishkori (S'10) received the B.Sc. degree in electrical engineering in 2002 from the University of Engineering and Technology Lahore, Pakistan and later on worked in the industry for almost five years. In August 2009, he received the M.Sc. degree (cum Laude) in electrical engineering from the Delft University of Technology, The Netherlands. Since November 2009, he has been with the circuits and systems group at the Faculty of Electrical Engineering, Mathematics and Computer Science of Delft University of Technology, The Netherlands, in pursuance of the Ph.D. degree. His research interests include compressive sampling (compressed sensing), signal processing for communications and wireless communications.

Geert Leus (F'12) received the electrical engineering degree and the Ph.D. degree in applied sciences from the Katholieke Universiteit Leuven, Belgium, in June 1996 and May 2000, respectively. Currently, Geert Leus is an "Antoni van Leeuwenhoek" Full Professor at the Faculty of Electrical Engineering, Mathematics and Computer Science of the Delft University of Technology, The Netherlands. His research interests are in the area of signal processing for communications. Geert Leus received a 2002 IEEE Signal Processing Society Young Author Best Paper Award and a 2005 IEEE Signal Processing Society Best Paper Award. He is a Fellow of the IEEE. Geert Leus was the Chair of the IEEE Signal Processing for Communications and Networking Technical Committee, and an Associate Editor for the IEEE TRANSACTIONS ON SIGNAL PROCESSING, the IEEE TRANSACTIONS ON WIRELESS COMMUNICATIONS, and the IEEE SIGNAL PROCESSING LETTERS. Currently, he is a member of the IEEE Sensor Array and Multichannel Technical Committee and serves as the Editor in Chief of the *EURASIP Journal on Advances in Signal Processing*.